Cell Reports
Article

AKAP-Anchored PKA Maintains Neuronal L-type Calcium Channel Activity and NFAT Transcriptional Signaling

Jonathan G. Murphy,[1,2] Jennifer L. Sanderson,[1] Jessica A. Gorski,[1] John D. Scott,[3,4] William A. Catterall,[4] William A. Sather,[1,2] and Mark L. Dell'Acqua[1,2,*]
[1]Department of Pharmacology
[2]Neuroscience Program
Anschutz Medical Campus, University of Colorado School of Medicine, Aurora, CO 80045, USA
[3]Howard Hughes Medical Institute
[4]Department of Pharmacology
University of Washington School of Medicine, Seattle, WA 98195, USA
*Correspondence: mark.dellacqua@ucdenver.edu
http://dx.doi.org/10.1016/j.celrep.2014.04.027

SUMMARY

L-type voltage-gated Ca^{2+} channels (LTCC) couple neuronal excitation to gene transcription. LTCC activity is elevated by the cyclic AMP (cAMP)-dependent protein kinase (PKA) and depressed by the Ca^{2+}-dependent phosphatase calcineurin (CaN), and both enzymes are localized to the channel by A-kinase anchoring protein 79/150 (AKAP79/150). AKAP79/150 anchoring of CaN also promotes LTCC activation of transcription through dephosphorylation of the nuclear factor of activated T cells (NFAT). We report here that the basal activity of AKAP79/150-anchored PKA maintains neuronal LTCC coupling to CaN-NFAT signaling by preserving LTCC phosphorylation in opposition to anchored CaN. Genetic disruption of AKAP-PKA anchoring promoted redistribution of the kinase out of postsynaptic dendritic spines, profound decreases in LTCC phosphorylation and Ca^{2+} influx, and impaired NFAT movement to the nucleus and activation of transcription. Thus, LTCC-NFAT transcriptional signaling in neurons requires precise organization and balancing of PKA and CaN activities in the channel nanoenvironment, which is only made possible by AKAP79/150 scaffolding.

INTRODUCTION

In excitable cells, the $Ca_V1.1$–$Ca_V1.4$ family of L-type voltage-gated Ca^{2+} channels is indispensable for an array of cellular processes including muscle contraction, insulin secretion, neurotransmitter release, and transcriptional regulation (Catterall, 2011). Of particular interest here, postsynaptic L-type voltage-gated Ca^{2+} channels (LTCCs) serve a privileged role in coupling neuronal excitation to changes in gene expression. This coupling occurs by initiating Ca^{2+}-dependent kinase- and phosphatase-signaling pathways that activate transcription factors, including the NFATc1–NFATc4 family (Bading et al., 1993; Dolmetsch et al., 2001; Graef et al., 1999; Mermelstein et al., 2000; Murphy et al., 1991; Oliveria et al., 2007; Ulrich et al., 2012). It is well established that long-lasting forms of synaptic plasticity underlying learning and memory require gene transcription and protein synthesis (Greer and Greenberg, 2008; Kelleher et al., 2004). Moreover, $Ca_V1.2$ LTCC excitation-transcription coupling is necessary for important forms of long-term synaptic potentiation and learning and memory mediated by the hippocampus and other brain regions (Grover and Teyler, 1990; Langwieser et al., 2010; Moosmang et al., 2005). In keeping with these important neuronal functions, polymorphisms in the gene encoding $Ca_V1.2$ are linked to multiple neuropsychiatric disorders (Smoller et al., 2013). Thus, it is important to understand how neuronal LTCC activity and downstream signaling to the nucleus are regulated.

It is now recognized that the rate and spatial precision of phosphorylation and dephosphorylation reactions in cells are constrained through the anchoring of kinases and phosphatases near their targets by scaffold proteins (Wong and Scott, 2004). In particular, subcellular targeting by AKAP79/150 of the kinase PKA, phosphatase CaN (also known as PP2B and PPP3), and other enzymes promotes highly localized signaling events at the postsynaptic membrane of neuronal dendritic spines (note: AKAP150 is the rodent ortholog of human AKAP79) (Sanderson and Dell'Acqua, 2011). Importantly, AKAP79/150, PKA, CaN, and $Ca_V1.2$ exhibit an enrichment and colocalization in dendritic spines of hippocampal neurons (Di Biase et al., 2008; Gomez et al., 2002; Hell et al., 1996). Neuronal membrane depolarization initiates NFAT signaling by triggering Ca^{2+} influx through LTCCs to activate calmodulin (CaM) molecules tethered to the intracellular C-terminal domain of the channel (Peterson et al., 1999; Zühlke et al., 1999). Ca^{2+}-CaM promotes rapid activation of CaN, which is recruited to the LTCC through AKAP79/150 anchoring (Oliveria et al., 2007, 2012; Zhang and Shapiro, 2012). Organization of the LTCC-AKAP-CaN macromolecular complex at the plasma membrane arises in part through additional interaction of modified leucine zipper (LZ) motifs on

AKAP79/150 and the C-terminal tail of $Ca_V1.2$ (Hulme et al., 2003; Oliveria et al., 2007). Upon dissociation from the AKAP, Ca^{2+}-CaM-CaN dephosphorylates NFAT to expose nuclear localization sequences (NLS), facilitating NFAT translocation from the cytoplasm to the nucleus, where it binds to promoter DNA elements and controls transcription (Hogan et al., 2003; Li et al., 2012).

In addition to CaN, AKAP79/150 anchors PKA near the LTCC to promote phosphorylation-mediated enhancement of channel activity that is opposed by CaN dephosphorylation, likely through modification of serine residues in the $Ca_V1.2$ C terminus (De Jongh et al., 1996; Fuller et al., 2010; Gao et al., 1997; Hall et al., 2007; Oliveria et al., 2007, 2012). Thus, AKAP-anchored CaN paradoxically serves as both a negative feedback regulator of LTCC activity and a positive downstream transducer of LTCC Ca^{2+} signaling to NFAT. Modulation of LTCC activity by PKA has primarily been studied in the context of β-adrenergic enhancement of channel currents in the heart resulting from cyclic AMP (cAMP) elevations during the fight-or-flight response (Catterall, 2011). However, basal PKA activity could also play important regulatory roles in the context of AKAP-anchored complexes, where PKA catalytic subunits have intimate access to substrate proteins, even in the absence of cAMP stimulation, but surprisingly, the role of AKAP79/150-anchored PKA in controlling basal LTCC phosphorylation and signaling activity has not been directly investigated. Here and in a companion paper (Dittmer et al., 2014), we provide evidence that maintenance of basal LTCC phosphorylation and function in hippocampal neurons critically depends on AKAP79/150-anchored PKA opposing anchored CaN activity. Importantly, we also demonstrate a requirement for AKAP79/150-PKA anchoring in promoting effective neuronal LTCC coupling to CaN-NFAT signaling. Thus, LTCC-NFAT signaling in neurons requires precise organization and a proper balance of PKA and CaN activities in the L-channel nanoenvironment, which is made possible by AKAP79/150 scaffolding.

RESULTS

Characterization of a PKA-Anchoring Deficient AKAP150ΔPKA Mouse Model

For the present study, we developed an AKAP150 mouse model that allows us to discriminate the functions of AKAP150-PKA anchoring. The AKAP150 knockout mouse model, though useful, lacks utility for clearly determining the contribution of PKA in the context of a multivalent scaffold that also interacts with many other signaling enzymes, including CaN (Tunquist et al., 2008; Weisenhaus et al., 2010). Moreover, a previously developed AKAP150D36 knockin mouse, with a 36 amino acid C-terminal truncation, although unable to anchor PKA (Lu et al., 2007), also lacks the AKAP-modified LZ domain that interacts with $Ca_V1.2$ (Oliveria et al., 2007). Therefore, we engineered a targeted internal deletion in the *Akap5* gene to create an exclusively PKA-anchoring deficient AKAP150ΔPKA knockin mouse, which retains the C-terminal LZ domain. Specifically, the *Akap5*ΔPKA targeting vector deleted 30 bp encoding residues 709–718 within the amphipathic α-helical domain that anchors the PKA-RII regulatory subunit dimer and also inserted a C-terminal myc epitope tag after the LZ domain (Figures 1A and 1B). Importantly, the AKAP150ΔPKA deletion leaves intact all other AKAP structural domains, including those for CaN anchoring, adenylyl cyclase (AC) binding, and membrane targeting (Figure 1B) (Sanderson and Dell'Acqua, 2011).

The presence of the targeted *Akap5*ΔPKA allele in heterozygous and homozygous AKAP150ΔPKA mice was confirmed by PCR-based genotyping compared to wild-type (WT) (Figure 1C). Expression of AKAP150ΔPKA protein in homozygous mice was confirmed by immunoblotting to detect the engineered C-terminal myc tag (Figure 1D), and anti-AKAP150 immunoblotting showed that AKAP150 ΔPKA and WT proteins were expressed at equal levels in hippocampal extracts (Figures 1D and 1E). Importantly, immunoprecipitation revealed loss of PKA-RII regulatory and PKA-C catalytic subunits from the AKAP complex for 150ΔPKA extracts, as also seen in controls using extracts prepared from AKAP150$^{-/-}$ knockout mice (KO) (Figures 1D and 1E). As expected, immunoprecipitation of the CaNA catalytic subunit with AKAP150 was maintained for the ΔPKA mutation, but not in extracts from AKAP150 KO mice (Figures 1D and 1E). We also developed an analogous ΔPKA mutant by removal of amino acids 391–400 of the human ortholog AKAP79 (Figure 1B). Transfection of fluorescently tagged AKAP79WT-cyan fluorescent protein (CFP) with PKA-RIIα-yellow fluorescent protein (YFP) into human embryonic kidney 293 (HEK293) cells resulted in distinct AKAP-RII colocalization at the plasma membrane (Figure 1F). In contrast, cells expressing AKAP79ΔPKA-CFP exhibited normal membrane localization of AKAP79ΔPKA but a clear loss of PKA-RII-YFP membrane association (Figure 1F). To confirm that the ΔPKA mutation does not disrupt the C-terminal LZ interaction with the LTCC, we cotransfected either AKAP79 WT or ΔPKA-CFP with N- or C-terminally YFP-tagged $Ca_V1.2$ and measured membrane-associated Förster resonance energy transfer (FRET) in living tsA201 cells as in our previous work characterizing the AKAP-$Ca_V1.2$ LZ interaction (Oliveria et al., 2007). Importantly, 79ΔPKA exhibited levels of FRET comparable to 79WT with both the C and N termini of $Ca_V1.2$ (Figures 1G–1J).

AKAP79/150 Anchoring Localizes PKA and CaN to Neuronal Dendritic Spines

We previously demonstrated that AKAP79 regulates PKA localization in dendritic spines by overexpressing a truncated AKAP79(1–360) construct similar to the AKAP150D36 mouse mutation (Lu et al., 2007; Smith et al., 2006). To address whether the more-precise AKAPΔPKA mutation impacts PKA spine targeting, we cotransfected rat hippocampal neurons with PKA-RIIα-CFP and CaNAα-YFP and either AKAP79 WT or ΔPKA tagged with mCherry (mCh) in conjunction with a previously characterized short hairpin interfering RNA (shRNAi) to suppress endogenous AKAP150 expression (Hoshi et al., 2005; Oliveria et al., 2007). As expected, AKAP79WT-mCh displayed prominent localization in spines (Figure 2A) with quantification of spine/dendrite shaft fluorescence ratios of ~2 indicating prominent spine enrichment (Figure 2B). Both PKA-RII-CFP (Figure 2C) and CaNA-YFP (Figure 2E) exhibited colocalization in spines with 79WT-mCh (Figure 2G); however, whereas CaNA showed similar spine/shaft enrichment as AKAP79 (Figure 2F), PKA-RII was more evenly distributed

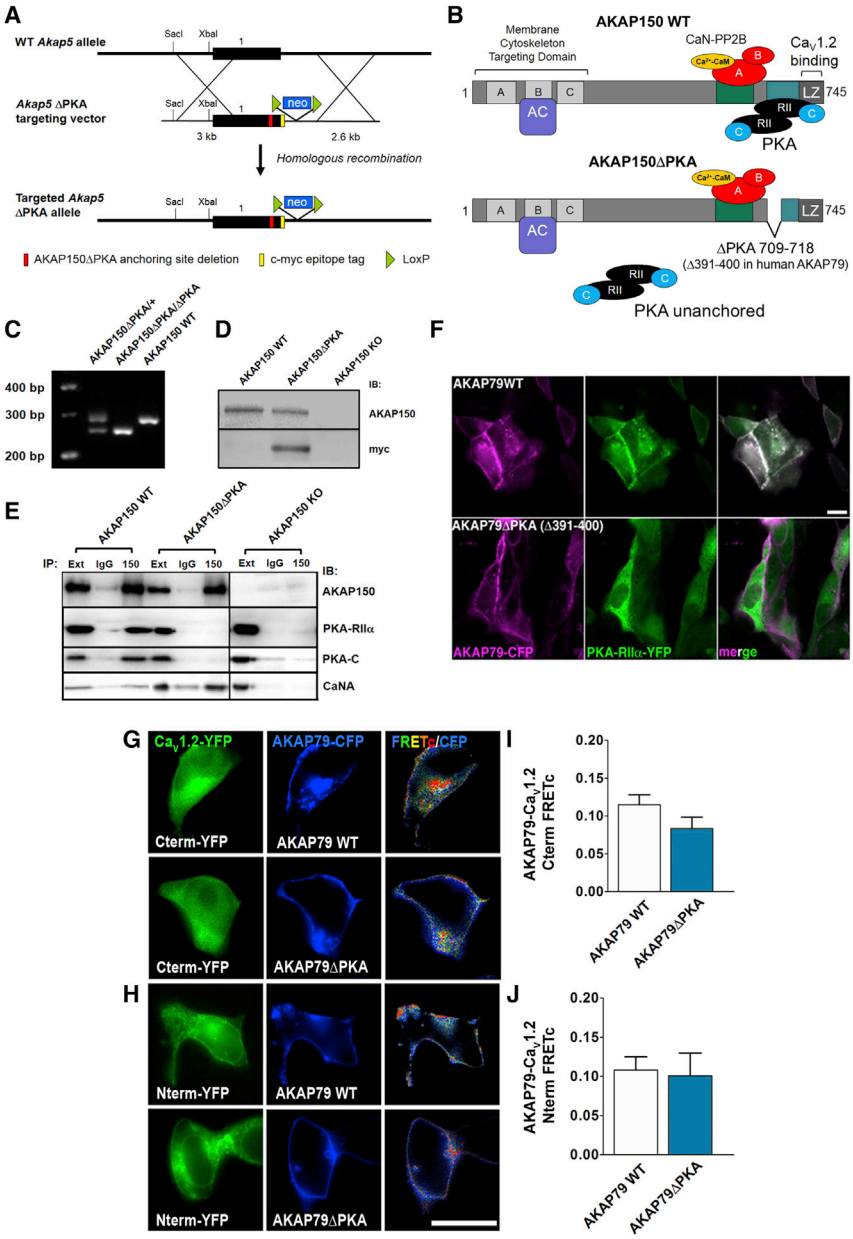

Figure 1. Characterization of PKA-Anchoring Deficient AKAP150ΔPKA Mice

(A) Diagram depicting the mouse *Akap5* gene encoding the AKAP150 WT allele (top), the targeting construct containing the ΔPKA mutation (middle), and the targeted ΔPKA allele (bottom). The single AKAP150 coding exon is represented by the black box. The red rectangle indicates the 30 bp encoding the ten amino acids of the ΔPKA deletion, yellow rectangle indicates the in-frame insertion of a c-*myc* epitope tag at the AKAP150 C terminus, and green triangles indicate loxP sites flanking the neomycin resistance cassette in the 3′ genomic DNA.

(B) Diagram of AKAP150 protein primary structure indicating removal of 709-LLIETASSLV-718 to selectively disrupt PKA-RII anchoring.

(C) PCR-based genotyping of WT and heterozygous and homozygous AKAP150ΔPKA littermate mice.

(D) Detection of AKAP150ΔPKA protein in whole-cell hippocampal extracts from homozygous mice by anti-myc and anti-AKAP150 immunoblotting (IB).

(E) The AKAP150ΔPKA mutation or AKAP150 KO (−/−) eliminates anti-AKAP150 coimmunoprecipitation of PKA-RII and C subunits. Ext, whole-cell hippocampal extract; IgG, immunoprecipitation (IP) with nonimmune immunoglobulin.

(F) HEK293 cells cotransfected with AKAP79 WT or ΔPKA-CFP (magenta) and PKA RII-YFP subunits (green). Colocalization appears white in the merged panel.

(G and H) tsA-201 cells cotransfected with C- or N-terminally tagged $Ca_V1.2$-YFP (FRET acceptor, green) and WT or ΔPKA AKAP79-CFP (FRET donor, blue). Corrected FRET (FRETc) shown in pseudocolor gated to CFP.

(I and J) Quantification of apparent FRET efficiency measured between $Ca_V1.2$-YFP and WT or ΔPKA AKAP79-CFP. Data expressed as mean ± SEM (not significantly different by t test; n = 7–17). The scale bars represent 10 μm.

between spines and the dendrite shaft with somewhat greater shaft localization (Figure 2F). AKAP79ΔPKA-mCh showed spine enrichment similar to 79WT (Figures 2A and 2B) but caused a loss of PKA-RII from spines (Figures 2C and 2D). Importantly, CaNA spine localization was unaffected by 79ΔPKA (Figures 2E and 2F). In contrast, an AKAP79ΔPIX mutant deleting the PxIxIT-like CaN-anchoring motif (Li et al., 2012; Oliveria et al., 2007) reduced CaN spine enrichment with no impact on PKA-RII localization (Figures 2E and 2F). Additionally, staining of endogenous AKAP150 and PKA-RIIβ in WT mouse neurons revealed spine enrichment of AKAP150 (Figures S1A and S1C) comparable to that observed for AKAP79 (Figures 2A and 2B) and spine enrichment of endogenous PKA-RIIβ (Figures S1A and S1B) even greater than that of overexpressed PKA-RIIα-CFP (Figures 2C and 2D), which is likely in excess of the number of available AKAP79/150-anchoring sites in spines as previously shown (Smith et al., 2006). In contrast, quantification of PKA-RII staining in AKAP150ΔPKA neurons revealed a nearly complete loss of PKA-RII spine localization (Figures S1A and S1B). Therefore, we conclude that AKAP79/150 targets both PKA and CaN to dendritic spines through their respective defined anchoring sites.

AKAP79/150 Anchoring of Both PKA and CaN Is Required for NFAT Translocation to the Neuronal Nucleus

As mentioned above, we previously described the importance of AKAP-CaN anchoring in mediating activation of NFAT by Ca^{2+}-CaN signaling initiated in the LTCC nanodomain (Li et al., 2012; Oliveria et al., 2007). To address the role of AKAP79/150-anchored PKA in NFAT signaling, we first transfected WT

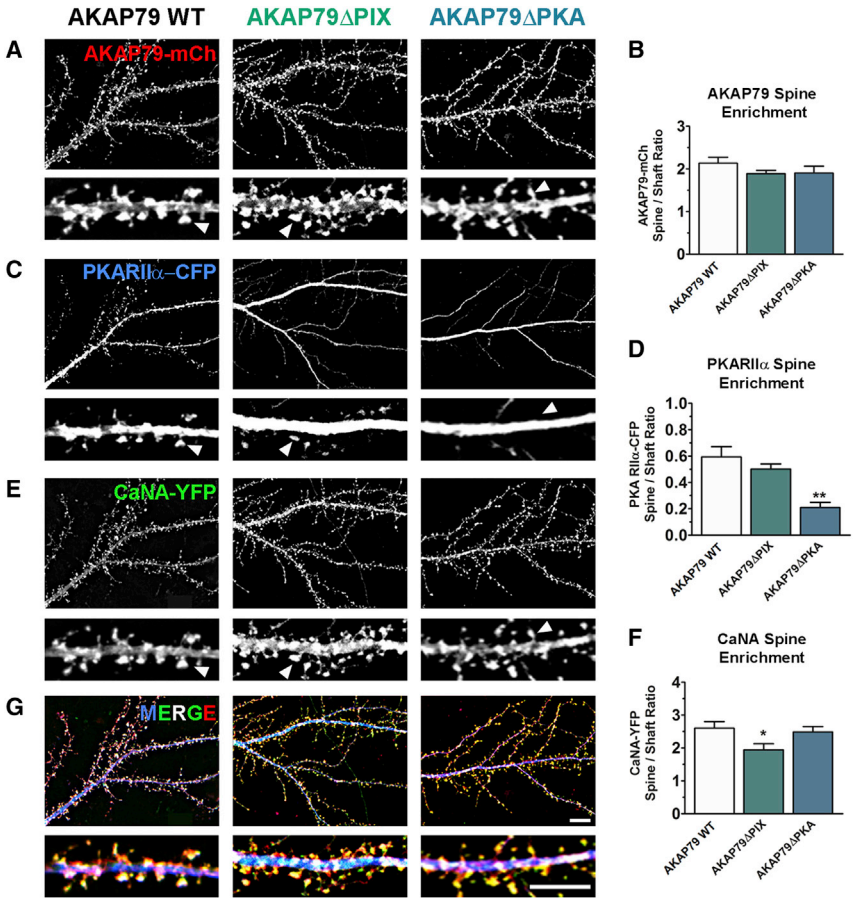

Figure 2. AKAP79/150 Anchoring Regulates CaN and PKA Localization to Dendritic Spines

(A) AKAP79 WT, ΔPIX, and ΔPKA-mCh localization in maximum intensity projection images of rat hippocampal neurons.

(B) Quantification of AKAP79-mCh WT and mutant dendritic spine localization as a spine/dendrite shaft fluorescence intensity ratio.

(C) AKAP79ΔPKA causes a loss of PKA-RIIα–CFP from spines relative to 79WT and 79ΔPIX.

(D) Quantification of PKA-RIIα-CFP spine/shaft ratios in neurons expressing WT or mutant AKAPs.

(E) AKAP79ΔPIX reduces spine localization of CaNA-YFP relative to WT and 79ΔPKA.

(F) Quantification of CaNAα-YFP spine/shaft ratios in neurons expressing WT or mutant AKAPs.

(G) Merged images of AKAP79-mCh, PKA-RIIα-CFP, and CaNAα-YFP in WT and mutant AKAP expressing neurons. Arrowheads indicate representative spines. Data expressed as mean ± SEM (*$p < 0.05$, **$p < 0.01$ by ANOVA with Dunnett's post hoc test; n = 18–23). The scale bars represent 10 μm.

mouse hippocampal neurons with NFATc3-GFP and induced nuclear translocation using a high-K^+ depolarization protocol that effectively activates LTCC excitation-transcription coupling (Graef et al., 1999; Oliveria et al., 2007; Wheeler et al., 2012; Figure 3A). As expected from previous work on NFAT in rat neurons (Graef et al., 1999; Oliveria et al., 2007; Ulrich et al., 2012), NFATc3-GFP accumulated densely in the nucleus 10 min after brief K^+ depolarization (Figures 3A and 3B) and then returned to the cytoplasm by 30 min (Figure 3A). This NFATc3 translocation was prevented by the dihydropyridine LTCC antagonist nimodipine, thus confirming the importance of LTCC Ca^{2+} entry in activation of the CaN-NFAT pathway (Figures 3B and 3C). Acute shRNAi-mediated knockdown of AKAP150 in rat neurons (Figures 3D and 3E) or genetic deletion of AKAP150 in mouse neurons (AKAP150 KO mice; Figures 3F and 3G) also strongly impaired K^+-stimulated NFATc3-GFP movement into the nucleus. Importantly, the effects of 150RNAi on NFATc3 were rescued by cotransfection of AKAP79 WT, but not by the ΔPIX mutant (Figures 3D and 3E). Neurons cultured from CaN-anchoring deficient AKAP150ΔPIX knockin mice (Sanderson et al., 2012) also showed attenuated NFATc3 accumulation in the nucleus (Figures 3F and 3G). This finding using NFATc3-GFP is consistent with previous work demonstrating a requirement for AKAP79/150-CaN anchoring in LTCC activation of endogenous NFATc4 (Li et al., 2012; Oliveria et al., 2007).

The interaction of PKA with multiple signaling targets makes it difficult to predict a specific role for AKAP79/150-anchored PKA in regulation of LTCC-NFAT signaling: PKA could act as a positive regulator of the upstream Ca^{2+} signal through LTCC phosphorylation and/or as a negative regulator of downstream nuclear import through NFAT phosphorylation. Previous studies showed that global inhibition of PKA activity increases NFAT nuclear accumulation in neurons and other cells (Belfield et al., 2006; Oliveria et al., 2007; Sheridan et al., 2002). However, anchoring of PKA to AKAP79/150 in the LTCC complex could favor one of these mechanisms. Indeed, in rat neurons expressing 150RNAi plus AKAP79ΔPKA (Figures 3D and 3E) and in neurons from AKAP150ΔPKA knockin mice (Figures 3F and 3G), we found that K^+-stimulated NFATc3-GFP nuclear translocation was strongly impaired, instead of being enhanced as previously observed with global PKA inhibition. In addition, we stimulated NFAT translocation by application of the dihydropyridine agonist BayK 8644 to promote LTCC activation during spontaneous neuronal firing: NFATc3-GFP nucleus/cytoplasm fluorescence increased ~22-fold in AKAP150 WT neurons compared to ~3-fold in ΔPIX and ~5-fold in ΔPKA knockin neurons (Figures S2A and S2B). Thus, disruption of either PKA or CaN anchoring to AKAP150, even in the presence of an LTCC agonist, greatly reduced NFAT activation. These results indicate that, when anchored by AKAP79/150, PKA acts only as a positive regulator of NFAT signaling.

AKAP79/150 Anchoring of PKA and CaN Is Required for NFAT Translocation out of Dendritic Spines

We next considered the possibility that NFAT may initially be localized near the LTCC-AKAP complex, within postsynaptic

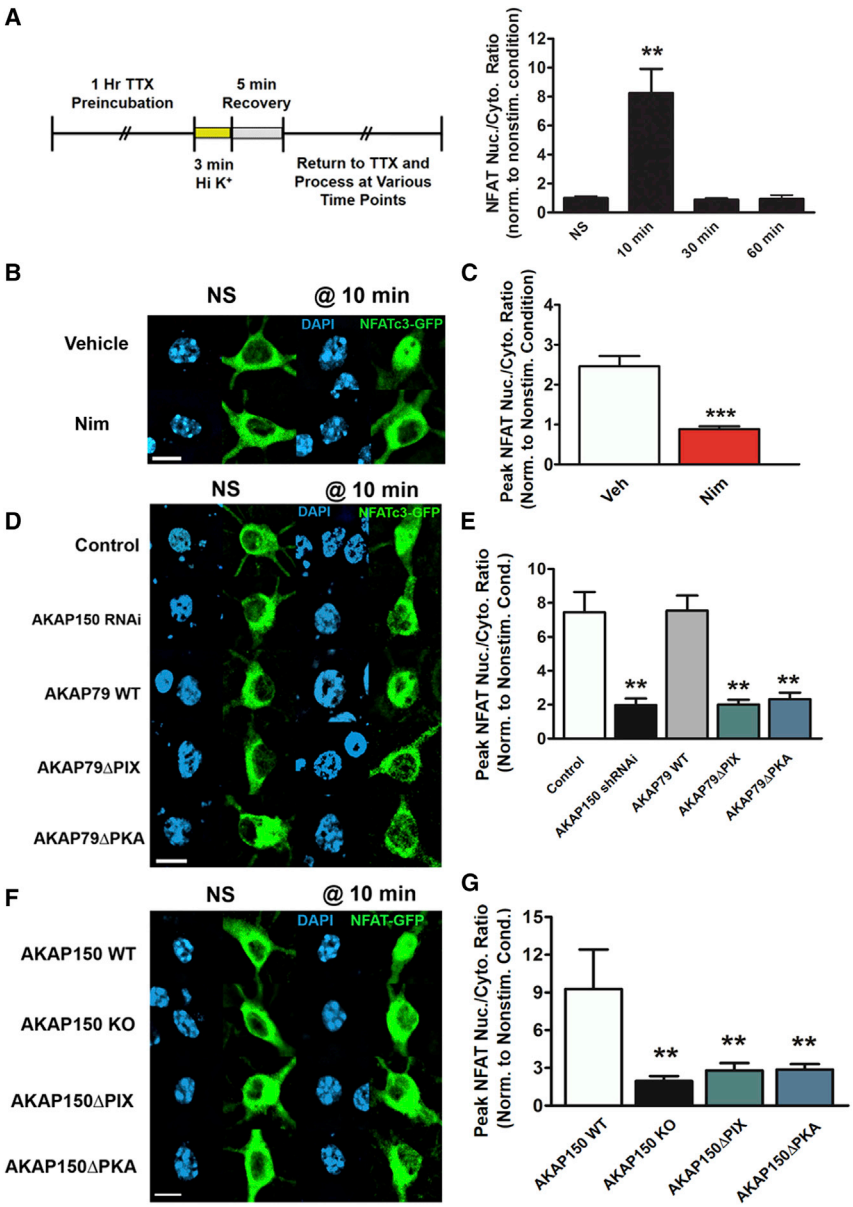

Figure 3. AKAP79/150 Anchoring of Both CaN and PKA Regulates Depolarization-Triggered NFAT Movement to the Nucleus in Hippocampal Neurons

(A) Schematic of the high-K^+ depolarization protocol (left) and quantification of NFATc3-GFP localization in the cytoplasm relative to the nucleus (nucleus/cytoplasm ratio) at the indicated times in control mouse hippocampal neurons (right).

(B) Summed intensity projection images of NFATc3-GFP (green) and nuclei (DAPI, blue) in WT mouse hippocampal neurons under nonstimulated (NS) conditions and 10 min after high-K^+ stimulation in DMSO (Vehicle) or nimodipine (Nim).

(C) Quantification of NFATc3-GFP translocation to nucleus 10 min after high-K^+ stimulation measured as the fold change in intrinsic GFP fluorescence nucleus/cytoplasm ratio relative to NS conditions.

(D) Images of NFATc3-GFP (anti-GFP, green) and nuclei (DAPI, blue) under NS conditions and 10 min after high-K^+ stimulation in rat neurons transfected with pSilencer empty vector (Control) or AKAP150 RNAi plus mCh alone, AKAP79-mCh WT, ΔPIX, or ΔPKA as indicated (mCh images not shown).

(E) Quantification of fold change in NFATc3-GFP immunostaining nucleus/cytoplasm ratio 10 min after high-K^+ stimulation relative to NS conditions.

(F) Hippocampal neurons from WT, AKAP150 KO, ΔPIX, or ΔPKA mice immunostained for NFATc3-GFP (green) and nuclei (DAPI, blue) under NS conditions and 10 min after a high-K^+ stimulation.

(G) Quantification of NFATc3-GFP nucleus/cytoplasm ratio for mouse neurons from (F) performed as in (E). Data expressed as mean ± SEM (**$p < 0.01$, ***$p < 0.001$; ANOVA with Dunnett's post hoc test or t test; n = 9–21). The scale bars represent 10 μm.

spines, and then departs spines in response to LTCC activation. To address this possibility, we measured the basal level of NFATc3 localization in spines. Not only did we observe NFATc3-GFP in spines, but we also observed a marked spine/shaft enrichment of NFATc3-GFP relative to cytoplasmic mCh, which was equally distributed between spines and dendrite shafts (Figures 4A–4C). Interestingly, 10 min after K^+ stimulation of control neurons, we measured a significant decrease in the spine/dendrite ratio for NFATc3-GFP, but mCh distribution was unchanged (Figures 4B and 4D). AKAP150 shRNAi knockdown prevented NFATc3 movement from spines, and this translocation defect was restored by co-expression of AKAP79 WT, but not ΔPIX or ΔPKA (Figure 4E). Thus, during the time frame that NFAT translocates to the nucleus (Figure 3A), NFAT also translocates out of dendritic spines, and both of these events depend on AKAP-anchored PKA and CaN. These findings are consistent with a significant fraction of NFAT that reaches the nucleus, having originated in spines where activating signals provided by the AKAP-LTCC complex are localized.

AKAP79/150 Anchoring of CaN and PKA Is Required for NFAT-Dependent Transcription

To address whether NFAT-dependent transcription is also defective in the absence of AKAP-PKA anchoring, we expressed a previously characterized 3xNFAT/AP1-CFPnls transcriptional reporter (Li et al., 2012) in neurons and measured the amount of CFP fluorescence sequestered in the nucleus following K^+ stimulation (Figures 5A–5C). Control rat neurons showed significantly higher nuclear CFP fluorescence 16 hr poststimulation, and AKAP150 shRNAi blocked this increase (Figures 5C and 5D). As seen for NFAT translocation,

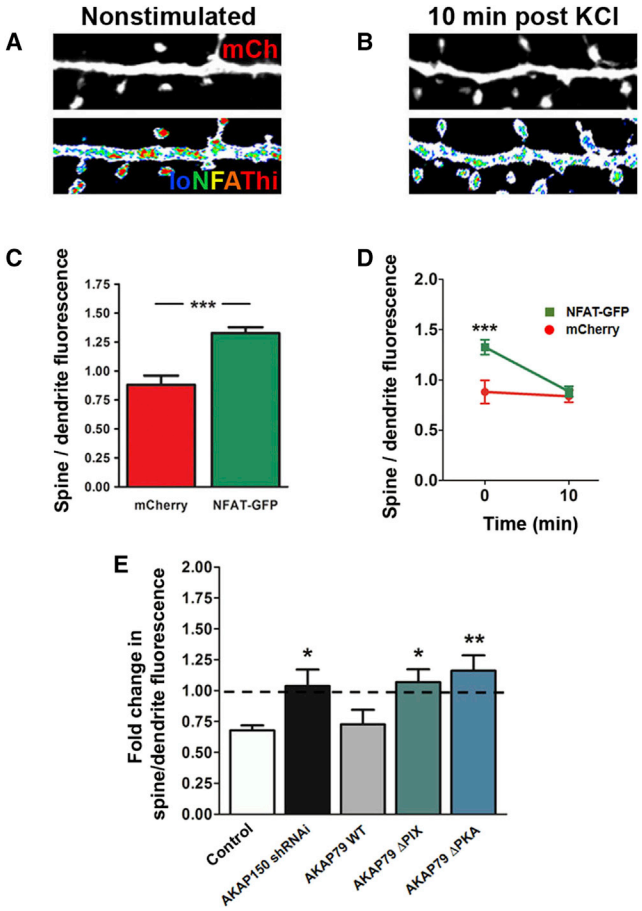

Figure 4. AKAP79/150 Anchoring of Both CaN and PKA Is Required for Depolarization-Triggered NFAT Translocation from Dendritic Spines

(A and B) Summed intensity projection images of control WT hippocampal neuron dendrites visualized by immunostaining of mCh (white) and overlaid by NFATc3-GFP immunostaining in pseudocolor with a relative scale from blue (low intensity) to red (high intensity). Images represent (A) nonstimulated conditions and (B) 10 min after high-K^+ stimulation.

(C–E) Quantification of mCh and NFATc3-GFP spine/dendrite shaft fluorescence ratios under basal conditions (C), following high-K^+ stimulation (D), and change from baseline (E) for conditions where AKAP79/150 expression and anchoring is altered as indicated. Data expressed as mean ± SEM (*$p < 0.05$, **$p < 0.01$, and ***$p < 0.001$ by paired t test or ANOVA with Dunnett's post hoc test compared to control; n = 5–19). The scale bars represent 10 μm.

coexpression of AKAP79 ΔPIX or ΔPKA with AKAP150 shRNAi failed to rescue the transcriptional deficit, whereas 79WT restored transcriptional activation to control levels (Figures 5C and 5D). Additionally, using a luciferase reporter of NFAT activity, we found transcriptional deficits in AKAP150 ΔPIX or ΔPKA knockin mouse neurons: at both 2 and 6 hr after high-K^+ depolarization, we observed a 4–5-fold increase in 3xNFAT/AP1-luciferase activity in WT neurons that was almost completely absent in neurons from AKAP150 ΔPIX and ΔPKA mice (Figures 5E and 5F).

AKAP79/150-Anchored CaN and PKA Control Basal Phosphorylation of $Ca_V1.2$

Taken together, our findings above show that AKAP79/150 anchoring of PKA and CaN are equally important for NFAT signaling, suggesting that the main function of anchored PKA in NFAT signaling may be as a positive regulator in phosphorylation-mediated control of LTCC function. Thus, for the AKAPΔPKA mutation, we hypothesized that LTCC hypophosphorylation may occur due to absence of anchored PKA in the channel nanodomain. To test this hypothesis, we immunoblotted extracts from AKAP150 WT, ΔPKA, ΔPIX, and KO hippocampal neurons to measure the amount of basal phosphorylation at two $Ca_V1.2$ Ser residues, S1700 and S1928, previously implicated in PKA regulation of LTCC function (De Jongh et al., 1996; Fuller et al., 2010; Gao et al., 1997; Oliveria et al., 2007). In AKAP150ΔPKA neurons, both S1700 and S1928 were significantly dephosphorylated compared to WT (Figures 6A–6C). Conversely, AKAP150ΔPIX mouse neurons showed equal levels of phosphorylation at S1700 and enhanced phosphorylation at S1928 (Figures 6A–6C). Interestingly, in AKAP150 KO neurons S1700 phosphorylation was reduced but S1928 phosphorylation was not different from WT (Figures 6A–6C). Overall, these findings suggest that AKAP79/150-anchored PKA maintains phosphorylation of S1700 in opposition to other phosphatases in addition to anchored CaN, whereas phosphorylation of S1928 is more tightly balanced by the opposed activities of AKAP79/150-anchored PKA and CaN. However, in AKAP150 KO neurons, where both PKA and CaN anchoring are disrupted, other pools of PKA or even other kinases, such as protein kinase C (Yang et al., 2005), may support basal S1928 phosphorylation.

Neuronal LTCC Ca^{2+} Influx Is Inhibited by Loss of AKAP79/150-PKA Anchoring

Our observations that AKAP79/150-PKA anchoring maintains basal $Ca_V1.2$ phosphorylation led us to investigate whether disruption of PKA anchoring also attenuates LTCC Ca^{2+} signals in hippocampal neurons. To measure Ca^{2+} signals, we carried out imaging in neurons transfected with the genetically encoded fluorescent Ca^{2+} indicator R-GECO1 (Zhao et al., 2011). We used the antagonist nimodipine to pharmacologically block the LTCC component of the Ca^{2+} signal evoked by K^+ depolarization and determined whether this component was altered under conditions of disrupted AKAP79/150 anchoring. When measured at the junction of the apical dendrite with the cell soma, a single 30 s high-K^+ perfusion elicited an ~4-fold increase in RGECO-1 fluorescence that rapidly returned to baseline in control rat neurons (Figures 7A–7D). In the presence of 10 μM nimodipine, this K^+-stimulated Ca^{2+} increase was reduced ~50% (Figure 7D). This ~50% LTCC contribution to the depolarization-induced Ca^{2+} signal is somewhat greater than observed in previous studies (20%–30%) using antidromic electrical stimulation, current recording, and Fura-2 calcium imaging (Christie et al., 1995; Hoogland and Saggau, 2004; Mermelstein et al., 2000; Regehr and Tank, 1992), consistent with K^+ depolarization leading to additional activation of postsynaptic glutamate receptors and Ca^{2+}-induced store release that can act both upstream and downstream to shape and amplify the LTCC contribution to the overall Ca^{2+} signal.

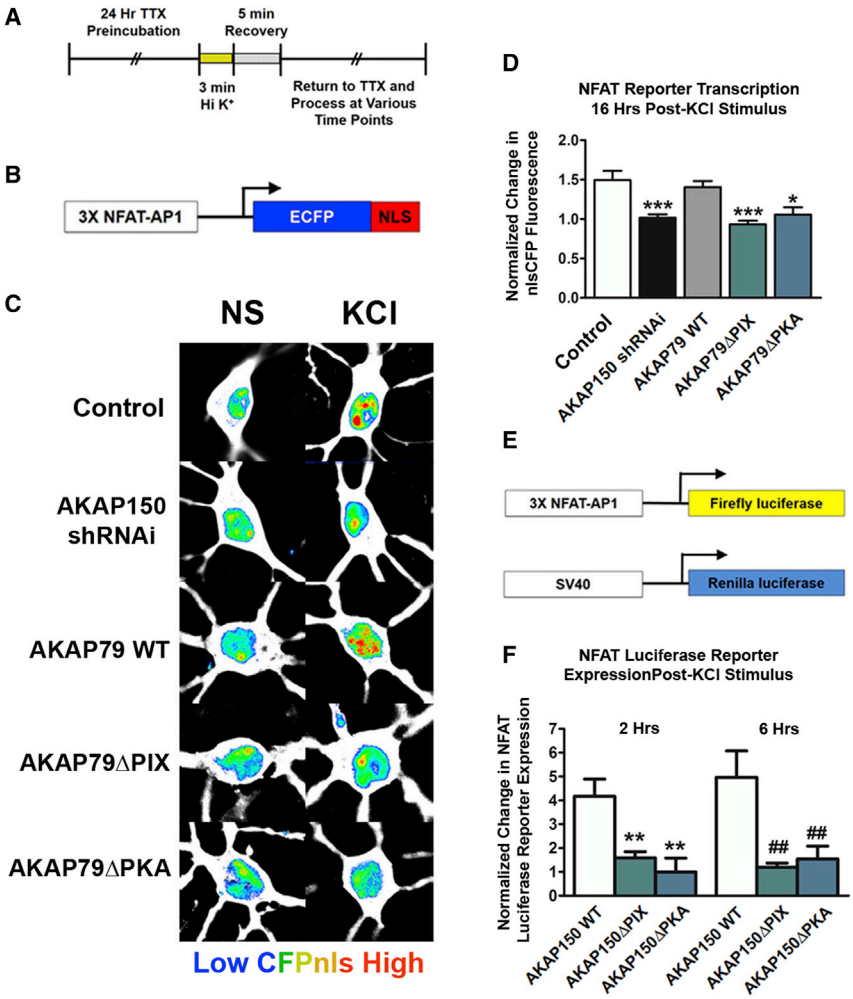

Figure 5. AKAP79/150 Anchoring of Both CaN and PKA Is Necessary for NFAT-Dependent Transcription

(A) Modified high-K^+ stimulation protocol for stimulation of NFAT-dependent transcription.

(B) Diagram of the 3xNFAT/AP1-CFPnls transcriptional reporter construct used for single-cell imaging of NFAT-dependent transcription.

(C) Summed intensity projection images of neuronal cell bodies and proximal dendrites in NS conditions and 16 hr after high-K^+ stimulation (KCl). Neurons were transfected with the 3xNFAT/AP1-CFPnls reporter along with pSilencer empty vector (Control) or 150RNAi plus YFP or the indicated AKAP79-YFP constructs. YFP fluorescence is in white, and nuclear-localized CFP fluorescence is in pseudocolor.

(D) Quantification of the fold change in nuclear fluorescence of the 3xNFAT-AP1-CFP-NLS reporter following high-K^+ stimulation for the indicated conditions.

(E) Diagram of the pGL3NFAT plasmid that drives NFAT-dependent transcription of firefly luciferase and the internal transfection control plasmid pRLSV40 driving constitutive transcription of *Renilla* luciferase.

(F) Quantification of NFAT-dependent transcription as normalized luciferase activity measured from lysates of WT and AKAP150 mutant mouse neurons. Data expressed as mean ± SEM (*$p < 0.05$, **,##$p < 0.01$, and ***$p < 0.001$ by ANOVA with Dunnett's post hoc test; n = 14–49 [rat]; n = 6–14 [mouse]). The scale bars represent 10 μm.

Importantly, following shRNAi knockdown of endogenous AKAP150 in rat neurons, the nimodipine-sensitive component of the Ca^{2+} signal was essentially eliminated (Figure 7E) but could be rescued by coexpression of human AKAP79WT-YFP (Figure 7F). The LTCC Ca^{2+} component in WT mouse neurons was nearly identical to that of control rat neurons with ~50% of the Ca^{2+} signal attributable to the LTCC (Figure 7H). AKAP150 KO mouse neurons exhibited no measureable LTCC component and displayed a reduced overall Ca^{2+} signal (Figure 7I) that was nearly identical to the reduction seen in AKAP150 shRNAi-expressing rat neurons (Figure 7E). In contrast, the LTCC component in AKAP150ΔPIX mouse neurons was maintained at a level similar to in WT neurons (Figure 7J), suggesting that loss of CaN anchoring, and the resulting increased basal S1928 phosphorylation (Figure 6), afforded no additional enhancement of LTCC function, at least in response to K^+ stimulation. However, AKAP150ΔPKA mouse neurons, like AKAP150 KO neurons, showed a clear loss of the LTCC component (Figure 7K). To confirm this large decrease in LTCC Ca^{2+} signaling in ΔPKA neurons, we performed additional imaging (Figure S3) using GCaMP6F, a Ca^{2+} indicator with even faster kinetics and higher sensitivity than RGECO-1(Chen et al., 2013). In agreement with findings above, in AKAP150 shRNAi rat neurons rescued with AKAP79WT-mCh, nimodipine strongly decreased the K^+-stimulated GCaMP6F Ca^{2+} signal (Figures S3A–S3D), but in neurons rescued with AKAP79ΔPKA-mCh, the total Ca^{2+} signal was already strongly reduced and nimodipine sensitivity was absent (Figures S3C and S3D). Using electrophysiological whole-cell recording, our companion paper (Dittmer et al., 2014) provides complementary evidence that LTCC current density in hippocampal neurons decreases when AKAP79/150-PKA signaling is disrupted. Thus, overall, our results indicate that loss of AKAP79/150-PKA anchoring leads to reduced basal LTCC phosphorylation and reduced depolarization-evoked Ca^{2+} influx that is insufficient to initiate effective CaN-NFAT signaling.

DISCUSSION

Our analysis of the AKAP79/150 ΔPKA mutant reveals that disruption of PKA anchoring uncouples downstream LTCC-CaN signaling to NFAT in hippocampal neurons as effectively as genetic disruption of CaN anchoring. Past and present work clearly shows that the phosphatase CaN must be targeted near the LTCC to provide efficient and specific activation of NFAT signaling via channel Ca^{2+} influx (Li et al., 2012; Oliveria et al., 2007; Zhang and Shapiro, 2012). Yet sequestering CaN within the LTCC nanodomain also promotes a robust

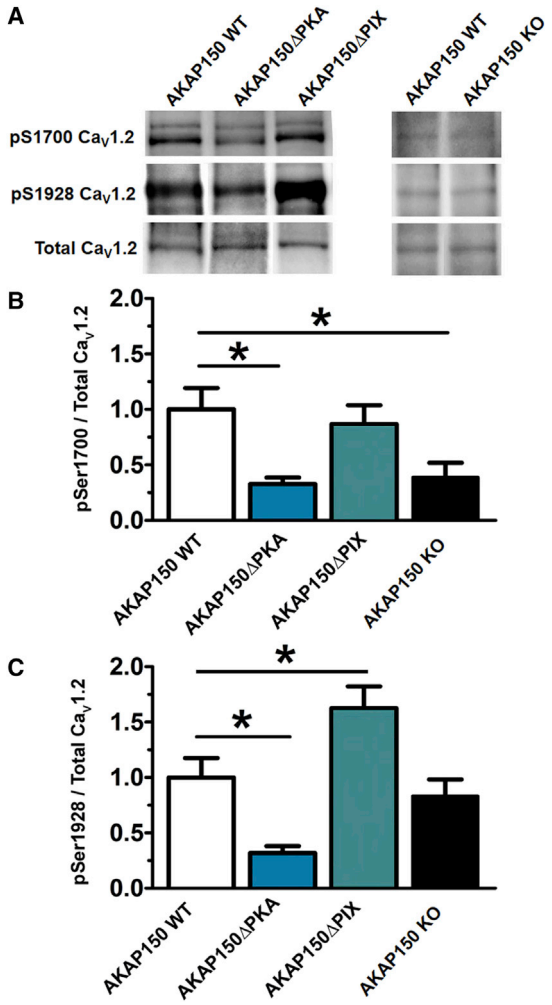

Figure 6. Anchoring of Both CaN and PKA to AKAP79/150 Regulates Basal Phosphorylation of $Ca_V1.2$

(A) Representative immunoblots of pS1700, pS1928, and total $Ca_V1.2$ from the indicated cultured mouse hippocampal neuron extracts.

(B) Quantification of $Ca_V1.2$ pS1928 over total $Ca_V1.2$ band intensity and normalized to WT.

(C) Quantification of $Ca_V1.2$ pS1700 over total $Ca_V1.2$ band intensity and normalized to WT. Data represented as mean ± SEM (*$p < 0.05$ by ANOVA with Dunnett's post hoc test; n = 4–5).

phosphatase-mediated negative feedback on PKA-enhanced channel activity, both through suppression of peak current amplitude and promotion of Ca^{2+}-dependent inactivation (CDI) of neuronal LTCCs (Dittmer et al., 2014; Oliveria et al., 2007, 2012). Indeed, whereas previous studies in hippocampal neurons demonstrated that LTCC current and Ca^{2+} influx can be enhanced by activation of cAMP-PKA signaling (Hoogland and Saggau, 2004; Kavalali et al., 1997), the degree of PKA enhancement of LTCC current is constrained by AKAP79/150-anchored CaN activity (Oliveria et al., 2007). Here, and in our companion paper (Dittmer et al., 2014), we discovered that, without coanchoring of PKA to balance CaN action in the LTCC nanodomain, even under basal conditions, phosphatase-mediated channel dephosphorylation becomes dominant, leading to disruption of CDI, depression of Ca^{2+} influx, and in turn a downstream Ca^{2+}-CaN signal insufficient to activate NFAT. Thus, overall, the opposing activity of PKA ends up working in conjunction with CaN to support NFAT signaling to the nucleus.

Interestingly, for AKAP79/150ΔPKA neurons, measurements of pharmacologically isolated LTCC currents in Dittmer et al. (2014) detected an ~40% reduction in current density, whereas imaging experiments here revealed an essentially complete loss of LTCC contributions to K^+-evoked Ca^{2+} transients. Due to necessary, inherent differences in experimental conditions, it is difficult to make absolute, quantitative comparisons between LTCC current measurements and LTCC contributions to global Ca^{2+} signals detected by imaging. For instance, to obtain accurate measurements of cell capacitance (proportional to cell size), LTCC current density measurements in Dittmer et al. (2014) were limited to immature 5-day-old cultured neurons that have not yet developed extensive dendritic arbors or spines. Thus, it is entirely possible that LTCC channel activity is decreased even more than 40% in the larger, more-mature, and spiny 12–15-day-old neurons we examined by Ca^{2+} imaging. Regardless of such developmental differences, it would also not be surprising if loss of AKAP-PKA anchoring had a much greater impact on the total K^+-evoked Ca^{2+} signal than on isolated LTCC currents due to even moderate reductions in channel Ca^{2+} influx being sufficient to disrupt effective coupling to other downstream Ca^{2+} sources, such as intracellular Ca^{2+} stores. In any case, multiple lines of evidence show that disruption of AKAP79/150-PKA anchoring leads to decreased LTCC Ca^{2+} signaling to CaN-NFAT.

Importantly, this key discovery that anchored PKA is essential for maintaining LTCC-NFAT signaling in neurons was only made possible by using genetic approaches that specifically disrupt AKAP79/150-PKA anchoring, as earlier studies using less-specific, acute pharmacologic treatments that globally inhibit PKA activity or anchoring to all AKAPs failed to observe negative impacts on NFAT activation (Belfield et al., 2006; Oliveria et al., 2007). As mentioned above, global PKA inhibition has the exact opposite effect on NFAT nuclear translocation compared to specific AKAP79/150-PKA-anchoring disruption, perhaps due to more-dominant impacts of inhibiting other pools of PKA that directly phosphorylate NFAT. In addition, it is possible that, whereas acute disruption of PKA anchoring with stearated peptides in previous work prevented further enhancement of LTCC function with cAMP stimulation (Oliveria et al., 2007), this manipulation did not disrupt PKA signaling in the AKAP79/150 complex completely enough or for a sufficient period of time to cause significant decreases in basal LTCC phosphorylation and function.

The substantial decreases in LTCC function in AKAP150-deficient and ΔPKA neurons seen here and in Dittmer et al. (2014) also indicate that other AKAPs known to associate with $Ca_V1.2$, such as AKAP15/18 (*Akap7* gene; Hulme et al., 2003) and MAP2 (Davare et al., 1999), were incapable of compensating for loss of AKAP150. AKAP150 KO and RNAi likely inhibit LTCC-NFAT signaling due to the combined effects of disruption of PKA and CaN scaffolding to the channel, thereby decreasing both the upstream Ca^{2+} signal and the efficiency of downstream CaN activation. Decreased LTCC function and S1700 phosphorylation in AKAP150 RNAi and KO neurons

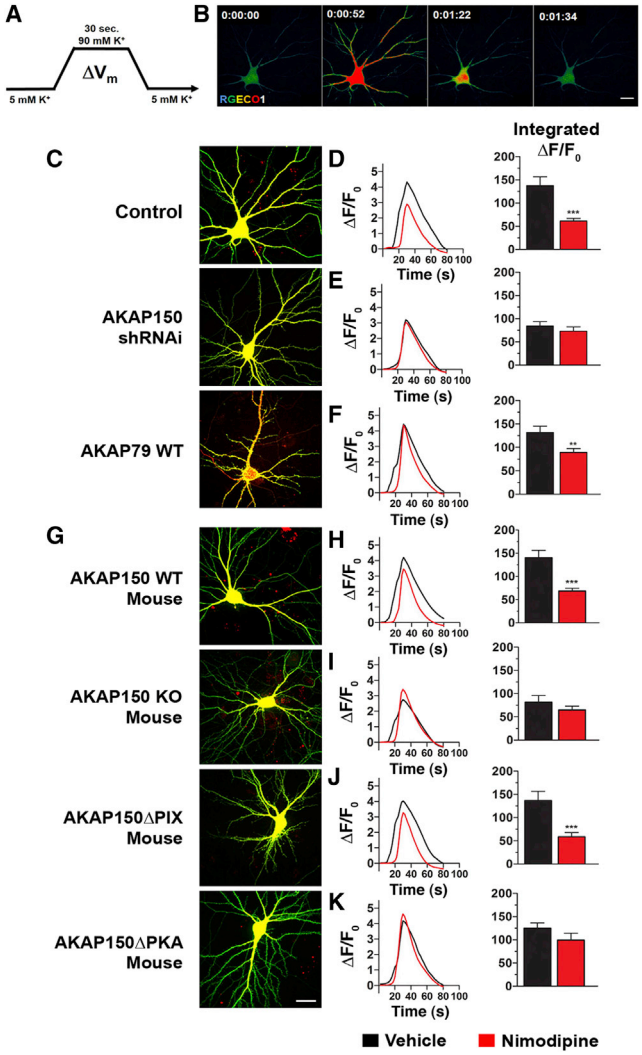

Figure 7. LTCC Ca^{2+} Signals Are Reduced in the Absence of AKAP79/150-PKA Anchoring

(A) Diagram of the high-K^+ depolarization protocol to trigger LTCC Ca^{2+} influx.

(B) Time course of RGECO-1 Ca^{2+}-indicator fluorescence change, shown in pseudocolor, in response to K^+ depolarization in control rat neurons.

(C) Representative live-cell images of rat hippocampal neurons expressing RGECO-1 (red) overlaid with YFP or AKAP79WT-YFP (green) prior to Ca^{2+} imaging.

(D–F) Time course (left panel) and quantification of area under the curve (right panel) for mean RGECO-1 fluorescence change over time in response to K^+ depolarization in rat neurons for the indicated conditions (Control = pSilencer empty vector).

(G) Representative live-cell images of WT and AKAP150 mutant mouse hippocampal neurons expressing RGECO-1 (red) overlaid with YFP (green) prior to Ca^{2+} imaging.

(H–K) Time courses (left panel) and quantification of integrated area under the response curve (right panel) for mean RGECO-1 fluorescence change over time in response to K^+ stimulation for WT and AKAP150 mutant mouse neurons. Data expressed as mean ± SEM (**p < 0.01, ***p < 0.001 by Student's t test; n = 11–18 [rat]; n = 9–16 [mouse]). The scale bars represent 10 μm.

cannot be due to anchored CaN activity unbalanced by anchored PKA activity (as in ΔPKA neurons) because CaN anchoring is also absent. Thus, the decreases in LTCC phosphorylation and function seen with AKAP150 RNAi and KO may instead be attributed to the known direct associations of CaN and PP2A with the $Ca_V1.2$ C terminus (Xu et al., 2010). However, in the context of either AKAP150 deficiency or the ΔPIX mutation, these direct PP2A and CaN interactions with $Ca_V1.2$ were unable on their own to suppress S1928 phosphorylation or to support CaN-NFAT signaling.

Whereas phosphorylation of S1700 and S1928 in the $Ca_V1.2$ C-terminal domain is implicated in PKA enhancement of LTCC currents, the functional roles of these two sites remain unclear. Nonetheless, for our purposes, S1700 and S1928 both served as valuable reporters of PKA and CaN activity in the AKAP-LTCC complex. We found that phosphorylation of these sites is correlated with effective signaling from the LTCC to the nucleus in neurons and that PKA anchoring to AKAP79/150 is required to maintain both phosphorylation and excitation-transcription coupling. Importantly, we also observed enhanced basal S1928 phosphorylation in AKAP150ΔPIX mouse neurons, and previous biochemical studies found impaired β-adrenergic stimulation of S1928 phosphorylation in brains of AKAP150 KO mice (Hall et al., 2007), thereby providing additional evidence that AKAP79/150-anchored PKA and CaN mediate bidirectional regulation of $Ca_V1.2$ phosphorylation in neurons. However, the specific functional roles of S1700 and S1928 in neuronal channel regulation await future investigation.

Our findings that genetic disruption of AKAP150-PKA anchoring strongly suppresses LTCC currents (Dittmer et al., 2014) and Ca^{2+} responses to K^+ stimulation are initially surprising but fit well with models first proposed over 25 years ago wherein L-channels must be phosphorylated by PKA to respond normally to membrane depolarization (Armstrong and Eckert, 1987). This required maintenance of basal channel phosphorylation could involve a combination of both cAMP-dependent and -independent signaling in the AKAP-LTCC complex. For example, AKAP79/150 also binds to several AC isoforms; hence, there may be local cAMP signaling tone that promotes basal PKA activity near the LTCC (Bauman et al., 2006; Willoughby et al., 2010). But basal phosphorylation of AKAP-linked substrates can also in part be mediated by cAMP-independent PKA activity (Smith et al., 2013). In any case, our present findings highlight that, in addition to orchestrating compartmentalized activation of PKA in response to cAMP elevations, maintenance of basal phosphorylation in subcellular nanodomains is another key function of AKAP scaffold proteins, especially when an opposing protein phosphatase is also anchored in the complex. Notably for neuronal function, this underappreciated aspect of AKAP regulation of basal PKA signaling is essential in priming LTCCs for effective excitation-transcription coupling through a phosphatase-signaling pathway coordinated by the same AKAP complex.

EXPERIMENTAL PROCEDURES

Generation of AKAP150ΔPKA Knockin Mice

The ΔPKA mutation, which removes 30 bp encoding 709-LLIETASSLV-718, was introduced into the single coding exon of an *Akap5* genomic DNA

fragment subcloned from a C57BL/6 bacterial artificial clone. In this targeting vector, the ΔPKA mutation and a C-terminal myc-epitope tag were introduced with a neomycin resistance cassette flanked by loxP sites inserted into 3′ genomic DNA. The targeting construct was electroporated into a hybrid C57BL/6-129 embryonic stem cell, and G418-resistant clones were screened for homologous recombinants by PCR-based genotyping. One positive clone was expanded, injected into blastocysts, and implanted into surrogate mothers. Chimeric F0 founders were born and bred to C57BL/6 to establish germ-line transmission. F1 mice heterozygous for the 150ΔPKA mutation were identified and then bred to yield F2 150ΔPKA homozygotes.

Primary Culture of Rodent Hippocampal Neurons

Mouse and rat hippocampal neurons were prepared as described previously (Gomez et al., 2002). Briefly, hippocampi were dissected from postnatal days 0–2 Sprague Dawley rats or AKAP150 WT, KO, ΔPIX, and ΔPKA mice. Neurons were plated at medium density (125,000 or 200,000 cells/ml) on poly-D-lysine alone (rat neurons) or also with laminin (mouse neurons) coated glass coverslips. Neurons were cultured in Neurobasal-A medium plus B-27 with mitotic inhibitors (Life Technologies) added at days in vitro (DIV) 4 or 5; thereafter, neurons were fed every 4 or 5 days.

Fluorescence Microscopy and Quantitative Image Analysis of Fixed Cells

Fluorescence images were captured using an Axiovert 200M microscope (Carl Zeiss) with a 63× plan-apo/1.4 numerical aperture (NA) objective, 300W xenon illumination (Sutter Instruments), Coolsnap-HQ2 charge-coupled device (CCD) camera (Roper Scientific), and Slidebook 4.2–5.5 software (Intelligent Imaging Innovations). AKAP79-mCh, CaNA-YFP, PKA-RII-CFP, NFAT-GFP, anti-AKAP150, and anti-PKA-RIIβ fluorescence was imaged by acquiring 2 μm z stacks of xy planes at 0.2 μm intervals. Planes were deblurred using nearest neighbors deconvolution and sum or maximum intensity projected into 2D images. Spine/dendrite shaft fluorescence ratios, NFAT translocation, and CFPnls transcriptional reporter activity were quantified as described previously (Li et al., 2012; Smith et al., 2006). Statistical comparisons of nucleus/cytoplasm ratios, spine/dendrite shaft ratios, and mean CFP fluorescence in the nucleus across groups were carried out using GraphPad Prism 4.0–5.0.

Live-Cell FRET Microscopy in tsA-201 Cells

tsA-201 cells were plated on glass coverslips in Dulbecco's modified Eagle's medium + 10% fetal bovine serum media, grown for 48 hr, and then transfected using Turbofect (Thermo Scientific) with cDNA plasmids encoding AKAP79 WT or ΔPKA-CFP and $Ca_V1.2$ Nterm-YFP or $Ca_V1.2$ Cterm-YFP as previously described (Oliveria et al., 2007). Living cells were imaged at room temperature 24–48 hr posttransfection using a Axiovert 200M microscope with a 63× plan-apo/1.4 NA objective, Lambda XL illumination (Sutter Instruments), Coolsnap-HQ CCD camera (Roper Scientific), and Slidebook 4.2–5.5 software. Three-filter FRET images were captured with 2 × 2 binning, processed, and apparent FRET efficiency measured as described previously (Oliveria et al., 2003, 2007).

Calcium Imaging in Hippocampal Neurons

Fast confocal imaging was performed using an EC Plan-Neofluar 40×/1.30 NA oil objective on an Axio-Observer Z1 microscope (Carl Zeiss) coupled to a CSU-X1 spinning disk (Yokogawa), an Evolve 16-bit electron-multiplying CCD camera (Photometrics), and Slidebook 5.0–5.5 software. DIV 12–15 neurons were grown on glass coverslips and transfected 24–48 hr prior to imaging. Neurons were transfected with pSilencer (empty vector control) or AKAP150 shRNAi; YFP, AKAP79 WT or ΔPKA-YFP/mCh, and RGECO-1 (Addgene 32444) or GCaMP6F (Addgene 40755) as indicated using Lipofectamine 2000 (Invitrogen). Following pretreatment with vehicle or nimodipine, coverslips were mounted in an imaging chamber (Warner Instruments; RC-21BDW) and perfused in normal Tyrode's saline containing TTX and vehicle or nimodipine for the duration of the experiment. Neurons were maintained at 34°C whereas single xy plane was acquired at 0.5 Hz for 1 or 2 min encompassing a 15 or 30 s 90 mM K^+ perfusion. Changes in RGECO-1/GCaMP6F fluorescence were measured for regions of interest at the base of a primary dendrite.

SUPPLEMENTAL INFORMATION

Supplemental Information includes Supplemental Experimental Procedures and three figures and can be found with this article online at http://dx.doi.org/10.1016/j.celrep.2014.04.027.

AUTHOR CONTRIBUTIONS

M.L.D., W.A.S., and J.G.M. designed the research. J.G.M. performed FRET imaging experiments in tsA201 cells, imaging of AKAP79/150, PKA, CaN, and NFAT localization, NFAT transcriptional reporter assays, analysis of $Ca_V1.2$ phosphorylation, and Ca^{2+} imaging in hippocampal neurons. J.L.S. prepared hippocampal neurons cultured from WT, AKAP150 $^{-/-}$, AKAP150ΔPKA, and AKAP150ΔPIX mice and characterized the AKAP79ΔPKA mutant in HEK293 cells. J.L.S. and J.A.G. characterized AKAP150ΔPKA mice by genotyping, immunoblotting, and coimmunoprecipitation. J.D.S. generated and provided AKAP150$^{-/-}$ mice. W.A.C. prepared, characterized, and provided $Ca_V1.2$ phospho-Ser1928 and phospho-Ser1700 antibodies. J.G.M. and M.L.D. wrote the manuscript with significant input from W.A.S., J.D.S., and W.A.C.

ACKNOWLEDGMENTS

We thank Andrew Thorburn and his laboratory for training in the use of the GloMax Multi Microplate Reader for luciferase experiments. This work was supported by grants from NIH to M.L.D. (R01MH102338, R01MH080291, and R01NS040701), J.D.S. (R01GM48231), and W.A.C. (R01HL085372). Imaging experiments were performed in the University of Colorado Anschutz Medical Campus Advanced Light Microscopy Core supported by NIH through the Rocky Mountain Neurological Disorders Core Center (P30NS048154) and by the Colorado CTSI (UL1TR001082). We thank Wallace Chick in the Rocky Mountain Neurological Disorders Core Center for constructing the Akap5ΔPKA targeting vector. Contents are the authors' sole responsibility and do not necessarily represent official NIH views.

Received: August 30, 2013
Revised: March 18, 2014
Accepted: April 15, 2014
Published: May 15, 2014

REFERENCES

Armstrong, D., and Eckert, R. (1987). Voltage-activated calcium channels that must be phosphorylated to respond to membrane depolarization. Proc. Natl. Acad. Sci. USA *84*, 2518–2522.

Bading, H., Ginty, D.D., and Greenberg, M.E. (1993). Regulation of gene expression in hippocampal neurons by distinct calcium signaling pathways. Science *260*, 181–186.

Bauman, A.L., Soughayer, J., Nguyen, B.T., Willoughby, D., Carnegie, G.K., Wong, W., Hoshi, N., Langeberg, L.K., Cooper, D.M., Dessauer, C.W., and Scott, J.D. (2006). Dynamic regulation of cAMP synthesis through anchored PKA-adenylyl cyclase V/VI complexes. Mol. Cell *23*, 925–931.

Belfield, J.L., Whittaker, C., Cader, M.Z., and Chawla, S. (2006). Differential effects of Ca2+ and cAMP on transcription mediated by MEF2D and cAMP-response element-binding protein in hippocampal neurons. J. Biol. Chem. *281*, 27724–27732.

Catterall, W.A. (2011). Voltage-gated calcium channels. Cold Spring Harb. Perspect. Biol. *3*, a003947.

Chen, T.W., Wardill, T.J., Sun, Y., Pulver, S.R., Renninger, S.L., Baohan, A., Schreiter, E.R., Kerr, R.A., Orger, M.B., Jayaraman, V., et al. (2013). Ultrasensitive fluorescent proteins for imaging neuronal activity. Nature *499*, 295–300.

Christie, B.R., Eliot, L.S., Ito, K., Miyakawa, H., and Johnston, D. (1995). Different Ca2+ channels in soma and dendrites of hippocampal pyramidal neurons mediate spike-induced Ca2+ influx. J. Neurophysiol. *73*, 2553–2557.

Davare, M.A., Dong, F., Rubin, C.S., and Hell, J.W. (1999). The A-kinase anchor protein MAP2B and cAMP-dependent protein kinase are associated with class C L-type calcium channels in neurons. J. Biol. Chem. *274*, 30280–30287.

De Jongh, K.S., Murphy, B.J., Colvin, A.A., Hell, J.W., Takahashi, M., and Catterall, W.A. (1996). Specific phosphorylation of a site in the full-length form of the alpha 1 subunit of the cardiac L-type calcium channel by adenosine 3′,5′-cyclic monophosphate-dependent protein kinase. Biochemistry *35*, 10392–10402.

Di Biase, V., Obermair, G.J., Szabo, Z., Altier, C., Sanguesa, J., Bourinet, E., and Flucher, B.E. (2008). Stable membrane expression of postsynaptic CaV1.2 calcium channel clusters is independent of interactions with AKAP79/150 and PDZ proteins. J. Neurosci. *28*, 13845–13855.

Dittmer, P.J., Dell'Acqua, M.L., and Sather, W.A. (2014). Ca^{2+}/Calcineurin-dependent inactivation of neuronal L-type Ca^{2+} channels requires priming by AKAP-anchored PKA. Cell Rep. *7*, this issue, 1410–1416.

Dolmetsch, R.E., Pajvani, U., Fife, K., Spotts, J.M., and Greenberg, M.E. (2001). Signaling to the nucleus by an L-type calcium channel-calmodulin complex through the MAP kinase pathway. Science *294*, 333–339.

Fuller, M.D., Emrick, M.A., Sadilek, M., Scheuer, T., and Catterall, W.A. (2010). Molecular mechanism of calcium channel regulation in the fight-or-flight response. Sci. Signal. *3*, ra70.

Gao, T., Yatani, A., Dell'Acqua, M.L., Sako, H., Green, S.A., Dascal, N., Scott, J.D., and Hosey, M.M. (1997). cAMP-dependent regulation of cardiac L-type Ca2+ channels requires membrane targeting of PKA and phosphorylation of channel subunits. Neuron *19*, 185–196.

Gomez, L.L., Alam, S., Smith, K.E., Horne, E., and Dell'Acqua, M.L. (2002). Regulation of A-kinase anchoring protein 79/150-cAMP-dependent protein kinase postsynaptic targeting by NMDA receptor activation of calcineurin and remodeling of dendritic actin. J. Neurosci. *22*, 7027–7044.

Graef, I.A., Mermelstein, P.G., Stankunas, K., Neilson, J.R., Deisseroth, K., Tsien, R.W., and Crabtree, G.R. (1999). L-type calcium channels and GSK-3 regulate the activity of NF-ATc4 in hippocampal neurons. Nature *401*, 703–708.

Greer, P.L., and Greenberg, M.E. (2008). From synapse to nucleus: calcium-dependent gene transcription in the control of synapse development and function. Neuron *59*, 846–860.

Grover, L.M., and Teyler, T.J. (1990). Two components of long-term potentiation induced by different patterns of afferent activation. Nature *347*, 477–479.

Hall, D.D., Davare, M.A., Shi, M., Allen, M.L., Weisenhaus, M., McKnight, G.S., and Hell, J.W. (2007). Critical role of cAMP-dependent protein kinase anchoring to the L-type calcium channel Cav1.2 via A-kinase anchor protein 150 in neurons. Biochemistry *46*, 1635–1646.

Hell, J.W., Westenbroek, R.E., Breeze, L.J., Wang, K.K., Chavkin, C., and Catterall, W.A. (1996). N-methyl-D-aspartate receptor-induced proteolytic conversion of postsynaptic class C L-type calcium channels in hippocampal neurons. Proc. Natl. Acad. Sci. USA *93*, 3362–3367.

Hogan, P.G., Chen, L., Nardone, J., and Rao, A. (2003). Transcriptional regulation by calcium, calcineurin, and NFAT. Genes Dev. *17*, 2205–2232.

Hoogland, T.M., and Saggau, P. (2004). Facilitation of L-type Ca2+ channels in dendritic spines by activation of beta2 adrenergic receptors. J. Neurosci. *24*, 8416–8427.

Hoshi, N., Langeberg, L.K., and Scott, J.D. (2005). Distinct enzyme combinations in AKAP signalling complexes permit functional diversity. Nat. Cell Biol. *7*, 1066–1073.

Hulme, J.T., Lin, T.W., Westenbroek, R.E., Scheuer, T., and Catterall, W.A. (2003). Beta-adrenergic regulation requires direct anchoring of PKA to cardiac CaV1.2 channels via a leucine zipper interaction with A kinase-anchoring protein 15. Proc. Natl. Acad. Sci. USA *100*, 13093–13098.

Kavalali, E.T., Hwang, K.S., and Plummer, M.R. (1997). cAMP-dependent enhancement of dihydropyridine-sensitive calcium channel availability in hippocampal neurons. J. Neurosci. *17*, 5334–5348.

Kelleher, R.J., 3rd, Govindarajan, A., and Tonegawa, S. (2004). Translational regulatory mechanisms in persistent forms of synaptic plasticity. Neuron *44*, 59–73.

Langwieser, N., Christel, C.J., Kleppisch, T., Hofmann, F., Wotjak, C.T., and Moosmang, S. (2010). Homeostatic switch in hebbian plasticity and fear learning after sustained loss of Cav1.2 calcium channels. J. Neurosci. *30*, 8367–8375.

Li, H.M., Pink, M.D., Murphy, J.G., Stein, A., Dell'Acqua, M.L., and Hogan, P.G. (2012). Balanced interactions of calcineurin with AKAP79 regulate Ca2+-calcineurin-NFAT signaling. Nat. Struct. Mol. Biol. *19*, 337–345.

Lu, Y., Allen, M., Halt, A.R., Weisenhaus, M., Dallapiazza, R.F., Hall, D.D., Usachev, Y.M., McKnight, G.S., and Hell, J.W. (2007). Age-dependent requirement of AKAP150-anchored PKA and GluR2-lacking AMPA receptors in LTP. EMBO J. *26*, 4879–4890.

Mermelstein, P.G., Bito, H., Deisseroth, K., and Tsien, R.W. (2000). Critical dependence of cAMP response element-binding protein phosphorylation on L-type calcium channels supports a selective response to EPSPs in preference to action potentials. J. Neurosci. *20*, 266–273.

Moosmang, S., Haider, N., Klugbauer, N., Adelsberger, H., Langwieser, N., Müller, J., Stiess, M., Marais, E., Schulla, V., Lacinova, L., et al. (2005). Role of hippocampal Cav1.2 Ca2+ channels in NMDA receptor-independent synaptic plasticity and spatial memory. J. Neurosci. *25*, 9883–9892.

Murphy, T.H., Worley, P.F., and Baraban, J.M. (1991). L-type voltage-sensitive calcium channels mediate synaptic activation of immediate early genes. Neuron *7*, 625–635.

Oliveria, S.F., Gomez, L.L., and Dell'Acqua, M.L. (2003). Imaging kinase—AKAP79—phosphatase scaffold complexes at the plasma membrane in living cells using FRET microscopy. J. Cell Biol. *160*, 101–112.

Oliveria, S.F., Dell'Acqua, M.L., and Sather, W.A. (2007). AKAP79/150 anchoring of calcineurin controls neuronal L-type Ca2+ channel activity and nuclear signaling. Neuron *55*, 261–275.

Oliveria, S.F., Dittmer, P.J., Youn, D.H., Dell'Acqua, M.L., and Sather, W.A. (2012). Localized calcineurin confers Ca2+-dependent inactivation on neuronal L-type Ca2+ channels. J. Neurosci. *32*, 15328–15337.

Peterson, B.Z., DeMaria, C.D., Adelman, J.P., and Yue, D.T. (1999). Calmodulin is the Ca2+ sensor for Ca2+ -dependent inactivation of L-type calcium channels. Neuron *22*, 549–558.

Regehr, W.G., and Tank, D.W. (1992). Calcium concentration dynamics produced by synaptic activation of CA1 hippocampal pyramidal cells. J. Neurosci. *12*, 4202–4223.

Sanderson, J.L., and Dell'Acqua, M.L. (2011). AKAP signaling complexes in regulation of excitatory synaptic plasticity. Neuroscientist *17*, 321–336.

Sanderson, J.L., Gorski, J.A., Gibson, E.S., Lam, P., Freund, R.K., Chick, W.S., and Dell'Acqua, M.L. (2012). AKAP150-anchored calcineurin regulates synaptic plasticity by limiting synaptic incorporation of Ca2+-permeable AMPA receptors. J. Neurosci. *32*, 15036–15052.

Sheridan, C.M., Heist, E.K., Beals, C.R., Crabtree, G.R., and Gardner, P. (2002). Protein kinase A negatively modulates the nuclear accumulation of NF-ATc1 by priming for subsequent phosphorylation by glycogen synthase kinase-3. J. Biol. Chem. *277*, 48664–48676.

Smith, K.E., Gibson, E.S., and Dell'Acqua, M.L. (2006). cAMP-dependent protein kinase postsynaptic localization regulated by NMDA receptor activation through translocation of an A-kinase anchoring protein scaffold protein. J. Neurosci. *26*, 2391–2402.

Smith, F.D., Reichow, S.L., Esseltine, J.L., Shi, D., Langeberg, L.K., Scott, J.D., and Gonen, T. (2013). Intrinsic disorder within an AKAP-protein kinase A complex guides local substrate phosphorylation. Elife *2*, e01319.

Smoller, J.W., Craddock, N., Kendler, K., Lee, P.H., Neale, B.M., Nurnberger, J.I., Ripke, S., Santangelo, S., and Sullivan, P.F.Cross-Disorder Group of the Psychiatric Genomics Consortium; Genetic Risk Outcome of Psychosis (GROUP) Consortium (2013). Identification of risk loci with shared effects on five major psychiatric disorders: a genome-wide analysis. Lancet *381*, 1371–1379.

Tunquist, B.J., Hoshi, N., Guire, E.S., Zhang, F., Mullendorff, K., Langeberg, L.K., Raber, J., and Scott, J.D. (2008). Loss of AKAP150 perturbs distinct neuronal processes in mice. Proc. Natl. Acad. Sci. USA *105*, 12557–12562.

Ulrich, J.D., Kim, M.S., Houlihan, P.R., Shutov, L.P., Mohapatra, D.P., Strack, S., and Usachev, Y.M. (2012). Distinct activation properties of the nuclear factor of activated T-cells (NFAT) isoforms NFATc3 and NFATc4 in neurons. J. Biol. Chem. *287*, 37594–37609.

Weisenhaus, M., Allen, M.L., Yang, L., Lu, Y., Nichols, C.B., Su, T., Hell, J.W., and McKnight, G.S. (2010). Mutations in AKAP5 disrupt dendritic signaling complexes and lead to electrophysiological and behavioral phenotypes in mice. PLoS ONE *5*, e10325.

Wheeler, D.G., Groth, R.D., Ma, H., Barrett, C.F., Owen, S.F., Safa, P., and Tsien, R.W. (2012). Ca(V)1 and Ca(V)2 channels engage distinct modes of Ca(2+) signaling to control CREB-dependent gene expression. Cell *149*, 1112–1124.

Willoughby, D., Masada, N., Wachten, S., Pagano, M., Halls, M.L., Everett, K.L., Ciruela, A., and Cooper, D.M. (2010). AKAP79/150 interacts with AC8 and regulates Ca2+-dependent cAMP synthesis in pancreatic and neuronal systems. J. Biol. Chem. *285*, 20328–20342.

Wong, W., and Scott, J.D. (2004). AKAP signalling complexes: focal points in space and time. Nat. Rev. Mol. Cell Biol. *5*, 959–970.

Xu, H., Ginsburg, K.S., Hall, D.D., Zimmermann, M., Stein, I.S., Zhang, M., Tandan, S., Hill, J.A., Horne, M.C., Bers, D., and Hell, J.W. (2010). Targeting of protein phosphatases PP2A and PP2B to the C-terminus of the L-type calcium channel Ca v1.2. Biochemistry *49*, 10298–10307.

Yang, L., Liu, G., Zakharov, S.I., Morrow, J.P., Rybin, V.O., Steinberg, S.F., and Marx, S.O. (2005). Ser1928 is a common site for Cav1.2 phosphorylation by protein kinase C isoforms. J. Biol. Chem. *280*, 207–214.

Zhang, J., and Shapiro, M.S. (2012). Activity-dependent transcriptional regulation of M-Type (Kv7) K(+) channels by AKAP79/150-mediated NFAT actions. Neuron *76*, 1133–1146.

Zhao, Y., Araki, S., Wu, J., Teramoto, T., Chang, Y.F., Nakano, M., Abdelfattah, A.S., Fujiwara, M., Ishihara, T., Nagai, T., and Campbell, R.E. (2011). An expanded palette of genetically encoded Ca^{2+} indicators. Science *333*, 1888–1891.

Zühlke, R.D., Pitt, G.S., Deisseroth, K., Tsien, R.W., and Reuter, H. (1999). Calmodulin supports both inactivation and facilitation of L-type calcium channels. Nature *399*, 159–162.

Cell Reports, Volume *7*

Supplemental Information

AKAP-Anchored PKA Maintains Neuronal L-type Calcium Channel Activity and NFAT Transcriptional Signaling

Jonathan G. Murphy, Jennifer L. Sanderson, Jessica A. Gorski, John D. Scott, William A. Catterall, William A. Sather, and Mark L. Dell'Acqua

Supplemental Material for Murphy et al., 2014 Cell Reports

Supplemental Figures

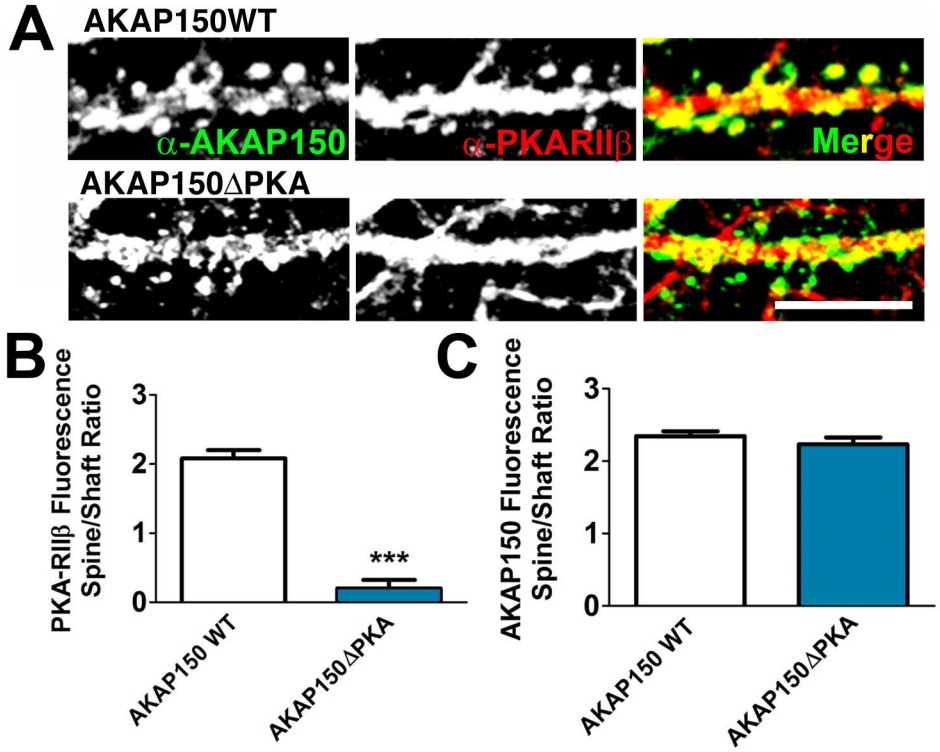

Figure S1 related to Figure 2

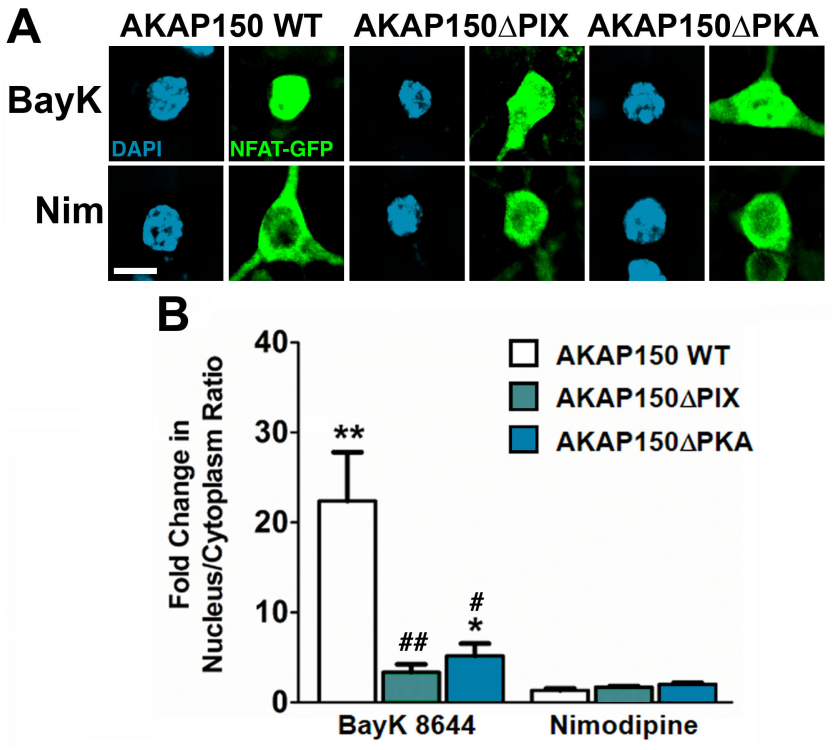

Figure S2 related to Figure 3

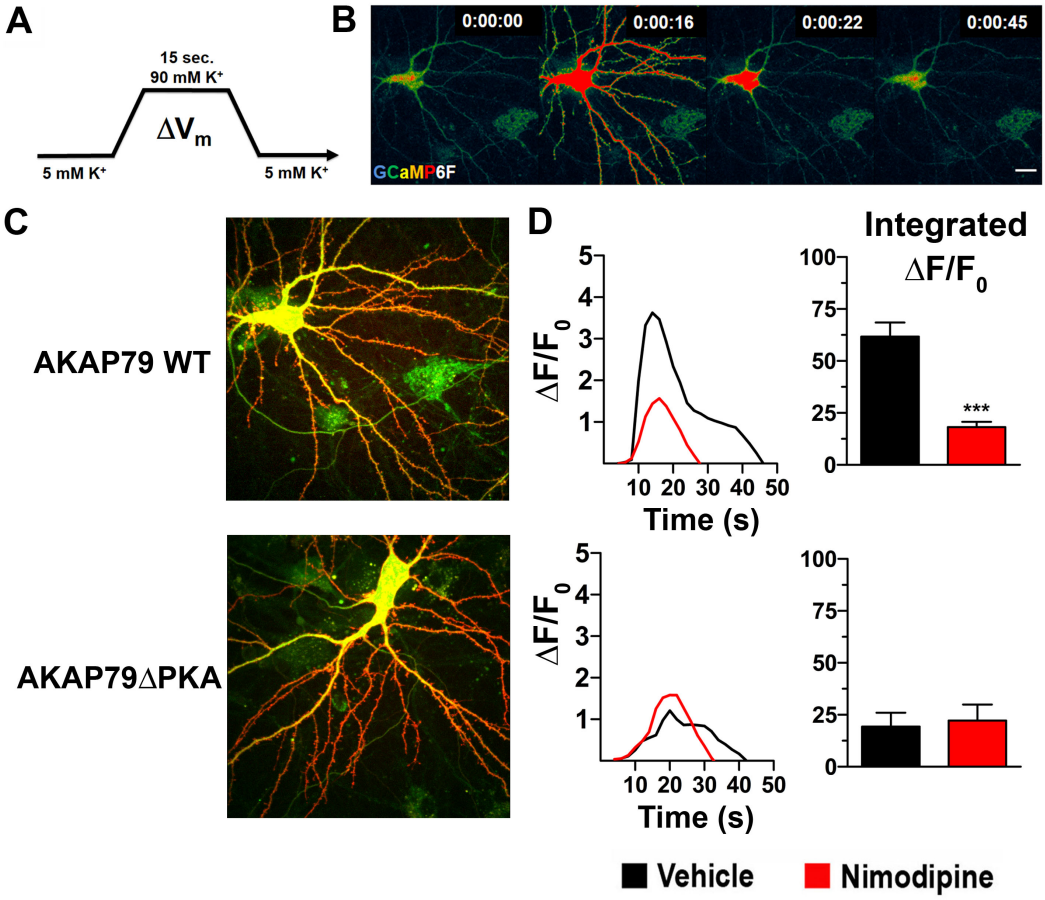

Figure S3 related to Figure 7

Supplemental Figure Legends

Figure S1 related to Figure 2: AKAP150 anchoring regulates PKA localization to dendritic spines. (A) Projection images of dendrite segments stained for AKAP150 (green) and PKA-RIIβ (red) for neurons from AKAP150 WT or ΔPKA knock-in mice showing reduced PKA-RIIβ localization in spines for AKAP150ΔPKA. (B) Quantification of PKA-RIIβ spine localization as a spine/dendrite shaft fluorescence intensity ratio for AKAP150 WT or ΔPKA knock-in mouse neurons. (C) Quantification of AKAP150 spine localization in AKAP150 WT or ΔPKA knock-in mouse neurons. Data expressed as mean ± SEM (***p<0.001by Student's t-test; n = 4-7). Scale bar = 10μm

Figure S2 related to Figure 3: AKAP79/150 anchoring of both CaN and PKA regulates NFAT movement to the nucleus in response to L-type Ca^{2+} channel opening driven by spontaneous neuronal activity. (A) Summed intensity projection images of NFATc3-GFP (green) and nuclei (DAPI, blue) in AKAP150 WT, AKAP150ΔPIX, and AKAP150ΔPKA mouse hippocampal neurons 10 min after TTX washout in the presence of BayK 8644 (BayK) to promote or nimodipine (Nim) to block LTCC activity. (B) Quantification of NFATc3-GFP translocation to nucleus 10 min after TTX washout measured as the fold-change in GFP fluorescence nucleus/cytoplasm ratio relative to non-stimulated conditions with no TTX washout (images not shown). Data expressed as mean ± SEM (*p<0.05, **p<0.01 compared to the corresponding Nim condition for that genotype by Student's t-test; $^{\#}$p<0.05, $^{\#\#}$p<0.01 compared to AKAP150 WT BayK stimulation by ANOVA with Bonferonni's Multiple Comparison Test; n = 5-12). Scale bar = 10μm

Figure S3 related to Figure 7: LTCC Ca^{2+} signals imaged with GCaMP6F are reduced in the absence of AKAP79/150-PKA anchoring. (A) Diagram of the high K^+ depolarization protocol to trigger LTCC Ca^{2+} influx. (B) Time-course of GCaMP6F Ca^{2+}-indicator fluorescence change, shown in pseudocolor, in response to K^+ depolarization in rat hippocampal neurons co-expressing AKAP150 shRNAi and AKAP79WT-mCh. (C) Representative live-cell images of GCaMP6F (green) overlaid on AKAP79WT-mCh or AKAP79ΔPKA-mCh (red) fluorescence prior to Ca^{2+} imaging in rat neurons also expressing AKAP150 shRNAi. (D) Time-course (left panel) and quantification of area under the curve (right panel) for mean GCaMP6F fluorescence change over time in response to K^+ depolarization in rat neurons for the indicated conditions Data expressed as mean ± SEM. (***p<0.001 by Student's t-test; n = 5-6). Scale bars = 10μm

Supplemental Experimental Procedures

Animal Care and Use

All animal procedures were conducted in accordance with National Institutes of Health (NIH)-United States Public Health Service guidelines and with the approval of the University of Colorado Denver Institutional Animal Care and Use Committee.

Mutant Mouse Genotyping and Husbandry

AKAP150 KO and AKAP150ΔPIX mice were genotyped and cared for as described previously (Sanderson et al., 2012; Tunquist et al., 2008). For PCR genotyping of AKAP150ΔPKA mice, DNA was extracted from tail tissue using REDExtract-N-Amp Tissue PCR kit (Sigma) following manufacturer's recommendations. PCR with forward (5'-ACCGAGATCAGAAGAAAGCAAACG-3') and reverse (5'-CCTCGGAAACCATTTCATTAACCA-3') primers amplified nucleotides 2282–2559 of the coding sequence, giving a 277 bp fragment for the WT allele and a 247 bp fragment for the ΔPKA allele. For most experiments, AKAP150ΔPKA mice were maintained on a mixed C57Bl6/129 background as heterozygous breeding pairs to provide WT littermate controls; however, for neonatal cultured neuron preparations, WT and ΔPKA homozygous breeding pairs were used to provide litters of a single genotype. AKAP150ΔPKA mice have no obvious alterations in physical, behavioral, or breeding phenotype in the home-cage environment.

Immunoprecipitation and Immunoblotting

AKAP150 immunoprecipitations (IP) from the hippocampus of ~2 month-old male and female mice were performed as per Gomez et al (Gomez et al., 2002) with slight modifications. Hippocampi were homogenized in lysis buffer (50 mM Tris pH 7.5, 0.15 M NaCl, 5 mM EDTA, 5 mM EGTA, 5 mM NaF, 2 mg/ml leupeptin, 2 mg/ml pepstatin, 1 mM Benzamidine and 1 mM

AEBSF), then incubated on ice for 20 min in the presence of 1% Triton X-100. Lysates were spun for 20 min at 20,800g. 10% of supernatant was reserved for gel loading. The remaining supernatant was diluted to 0.5% Triton X-100 and split evenly into two samples, receiving either 5 µg rabbit anti-AKAP150 or 5 µg rabbit anti-IgG antibodies. Samples were incubated for 4 hours at room temperature with end-over-end shaking, followed by one hour in protein A Sepharose beads, prior to extensive washing.

The entire immunoprecipitates or 15 µg whole extract (WE/input) were resolved on Tris-SDS gels and transferred in 20% methanol to PVDF membranes. 40 µg of WE was loaded gel for parallel blotting with anti-myc and anti- AKAP150. Primary antibodies were incubated with the membranes for a minimum of 90 min as follows: rabbit anti-AKAP150 (1:2000); (Brandao et al., 2012), mouse anti-myc and anti-PKA-RIIα (1:1000; Santa Cruz Biotechnology), mouse anti-PKA-C (1:1000; BD-Transduction Labs), and mouse anti-CaNA (1:1000; Sigma-Aldrich). Detection was performed with horseradish peroxidase (HRP)-coupled secondary antibodies (Bio-Rad; 1:1000) followed by enhanced chemiluminescence (ECL) (WestPico or West Dura Chemiluminescent Substrate; Pierce). Chemiluminescence was imaged using an Alpha Innotech Fluorchem gel documentation system.

Quantification of Live-cell FRET Microscopy in tsA-201 Cells

YFP, CFP and CYFRET fluorescence were detected in single xy planes in living cells to capture three images: 1) YFPexcitation/YFPemission, 2) CFP excitation/CFPemission, and 3) CFPexcitation/YFPemission (raw FRET). After background subtraction, fractional image subtraction corrected for CFP bleed-through and YFP cross-excitation,

FRETc = rawFRET – (0.54 x CFP) – (0,02 x YFP)

to yield an image of corrected FRET (FRETc), which was then gated to the CFP donor channel to create a FRETc/CFP pseudocolor image of relative FRET intensity in the cell**.** Mean CFP,

YFP, and raw FRET fluorescence intensities were measured by mask analysis of membrane regions (or the cytoplasm for linked CFP-YFP) in Slidebook 4.0-5.5 as described previously (Oliveria et al., 2003, Oliveria et al., 2007; Li et al., 2012). Apparent FRET efficiency (FRETeff) values were calculated from these mean intensities using the equation,

FRETeff = FRETc / ((0.02 x YFP) x 10.6)

for a 1:1 complex, where FRETc is the emission from YFP due to FRET, 0.02 * YFP is the emission from YFP directly excited with the FRET filter cube, 10.6 is a factor relating CFP excited to YFP excited with the FRET filter cube, and (0.02 * YFP) * 10.6 is therefore the maximum sensitized YFP emission possible if every excited CFP transferred its excitation to the associated YFP (Erickson et al., 2001; Erickson et al., 2003; Li et al., 2012; Oliveria et al., 2007).

Transfection of Rodent Primary Hippocampal Neurons

DIV 9-13 neurons were transfected using Lipofectamine 2000 (Life Technologies). Each transfection reaction contained 4-8 μg total plasmid encoding cDNA/shRNAi. For each 18 or 25 mm coverslip, either 4 or 8 μl of Lipofectamine was added, respectively. Briefly, NB and Lipofectamine or NB and plasmid DNA were combined incubated for 5 min in separate tubes at room temperature. After 5min, the Lipofectamine and DNA tubes were combined at room temperature and incubated for 20 min to create Lipofectamine/DNA complexes. During the 20-min incubaton time, half of the medium was removed from the cultured cells and mixed with fresh NB (+B27, +Glutamax) and saved. Following the 20-min incubation, the Lipofectamine/DNA mixture was added dropwise to the cultured neurons and allowed to incubate for 1.5-2.0 h at 37ºC, 5% CO_2. After incubation, Lipofectamine-containing media was replaced with conditioned culture media. Neurons were then returned to the incubator at 37ºC, 5% CO_2, and imaged within 2 days at DIV 10-14.

Quantification of AKAP79/150, CaNA, and PKA-RII Spine Enrichment

DIV12-14 cultured rat hippocampal neurons (24-48 hours post-transfection) were fixed for 10 min at room temperature with cold 3.7% paraformaldehyde in PBS and permeabilized for 10 min at room temperature in 0.1% TritonX-100 in PBS. Transfected rat neurons expressing AKAP-mCh, CaNAα-YFP, or PKA-RIIα-CFP were washed three times in PBS and mounted on glass slides with Pro-long Gold (Life Technologies). After fixation and permeabilization, cultured AKAP150 WT and ΔPKA knock-in mouse neurons were blocked in 3% BSA/PBS overnight at 4ºC. Primary antibodies (rabbit-anti-AKAP150 ((Brandao et al., 2012)) and mouse anti-PKA-RIIβ (R&D Systems)) were diluted 1:500 in 3% BSA/PBS, applied directly to coverslips, and incubated for 2 hrs at room temperature. After incubation with primary antibody, cells were washed 3x in PBS. Secondary antibodies (goat anti-rabbit Alexa Fluor 488 & goat anti-mouse Alexa Fluor 568, (Life Technologies)) were diluted 1:500 in 3% BSA/PBS, applied directly to coverslips, and incubated for 1 h at room temperature. Coverslips were then washed three times in PBS before mounting on glass slides with Pro-long gold. Measurements of spine fluorescence intensity were made by drawing masks using Slidebook 4.0-5.5 on all spines within the dendritic arbor in the field of view using a 63x, 1.4 NA Plan-apo objective and averaged for each neuron. Similarly, dendrite fluorescence intensity was measured by drawing masks over the dendrite shafts within the field of view and averaged into one number for each cell.

NFATc3-EGFP Translocation in Hippocampal Neurons

For rat neurons, DIV11-13 cultured hippocampal neurons (24-48 hours post-transfection) were placed in a Tyrode's salt solution including 1 μM TTX (Tocris) to dampen spontaneous activity and reduce basal levels of nuclear NFAT. Cells were incubated in Tyrode's + TTX at 37ºC, 5% CO_2, for 0.5 – 1.0 h. To block LTCCs, 10 μM nimodipine (Sigma-Aldrich) was applied 10 min prior to and throughout the TTX preincubation because of the use-dependence of

dihydropyridines. Subsequently, cells were depolarized for 3 min in isotonic 50 mM KCl Tyrode's solution to open LTCCs. Next, the cells were allowed to recover for 10 min in control Tyrode's solution containing 1 μM TTX at 37ºC, 5% CO_2. Cells then underwent immunocytochemistry to stain transfected NFATc3-GFP. After treatments, cultured hippocampal neurons were fixed, permeabilized, and stained as described above. Primary antibodies (mouse anti-GFP & rabbit anti-RFP, AbcaM) were diluted 1:500 in 3% BSA/PBS, applied directly to coverslips, and incubated for 2 hrs at room temperature. Cells were washed three times in PBS and secondary antibodies (goat anti-mouse Alexa Fluor 488 & goat anti-rabbit Alexa Fluor 568, Life Technologies) were diluted 1:500 in 3% BSA/PBS, applied directly to coverslips, and incubated for 1 h at room temperature. Coverslips were then washed three times in PBS before mounting on glass slides with Pro-long gold containing DAPI (Life Technologies).

Experiments in which spontaneous neuronal activity drives NFAT translocation were carried out as follows. After TTX pretreatment, neurons were washed two times over 5 min to remove residual TTX. Spontaneous activity in the neuron cultures then persisted for 10 min at 37°C in Tyrode's containing Vehicle (0.1% DMSO), BayK 8644 (10 μM), or nimodipine (10 μM). After treatments, cells were fixed, permeabilized, and stained as described above.

Measurement of NFAT Transcriptional Reporter Expression

NFAT transcriptional reporter assays were carried out essentially as described previously (Graef et al., 1999; Li et al., 2012). 12 DIV mouse hippocampal neurons were transfected with GL3NFAT firefly (Hedin et al., 1997) & RLSV40 *Renilla* luciferase plasmids. Alternatively, 12 DIV rat neurons were transfected with the 3xNFAT-AP1–CFP-NLS fluorescent reporter plasmid, pSilencer or AKAP150 shRNAi, and either YFP, AKAP79YFP WT or mutant plasmids as described above. 4h or 26 h after transfection (for 16 h or 6 h post-KCl conditions, respectively, to ensure in both cases that cDNA and RNAi constructs would be expressed for a total of ~2 days post-transfection before fixation) 1 μM TTX was added in conditioned NB culture medium for 24 h at 37ºC, 5% CO_2, to dampen spontaneous activity and decrease basal

CFP expression. After this TTX pretreatment, neurons were subjected to a 5 min wash in control Tyrode's followed by a 3 min depolarization with isotonic 50mM (mouse) or 90 mM (rat) KCl as above. Residual high K^+ was removed with an additional 5 min control Tyrode's wash and cells were returned to conditioned NB media containing 1 μM TTX for 6 or 16 h at 37ºC, 5% CO_2. Rat neurons expressing the 3xNFAT-AP1–CFP-NLS reporter were fixed in 3.7% formaldehyde in PBS, permeabilized with 0.05% Triton X-100 in PBS, stained with a 1 μM solution of propidium iodide (PI) to visualize the nucleus, and mounted onto glass slides as above. Mouse luciferase expression was measured in mouse cultures using the Dual Luciferase Reporter Assay System (Promega) and a GloMax Multi Microplate Reader (Promega). NFAT-dependent firefly luciferase signal was normalized to *Renilla* luciferase to correct for transfection and expression differences among cultures.

Phospho-Ca_v1.2 Western Blots

Primary hippocampal neurons from AKAP150 WT, ΔPIX, and ΔPKA mouse strains were cultured to DIV 12-16 in 6-well culture dishes and scraped into RIPA buffer (10.0 mM Tris pH 7.4, 100.0 mM NaCl, 5.0 mM EDTA, 5.0 mM EGTA, 1.0% Deoxycholate, 0.1% SDS, 1.0% Triton X-100) containing the protease inhibitors 1 μM AEBSF, 1 μM benzamidine, 1 μM calpain inhibitors I & II, 2 μg/ml leupeptin, 2 μg/ml pepstatin, and the phosphatase inhibitors cyclosporine A, 1 μM microcystin, 5 mM NaF, and 2 mM Na_3VO_4. Each batch of cultured neurons were then lysed using a Dounce homogenizer. Extracts were cleared by centrifugation (20,800g) at 4°C for 20 min and stored at -80°C until immunoblotting. Prior to gel loading, samples were heated to 65°C for 20 min in sample buffer (62.5 mM Tris-HCl pH 6.8, 10.0 % glycerol, 5.0 % β-mercaptoethanol, 2.0% SDS, 0.025 % Bromophenol blue). 20μg of total extract protein was electrophoresed through Tris-SDS gels and transferred to PVDF membranes in 7.5% methanol. Blots were blocked for 1 hr at room temperature. Primary Ca_V1.2 antibodies were diluted 1:500 in 3% BSA/TBS-T (rabbit anti-Ca_V1.2 pS1700 (Fuller et al., 2010), rabbit anti-Ca_V1.2 pS1928 (De Jongh et al., 1996), and mouse anti-Ca_V1.2 (Neuromabs, clone

L57/46). Following 3x5min TBS-T washes, blots were incubated with goat α-mouse or goat α-rabbit horseradish peroxidase (HRP) conjugated secondary antibodies (Bio-Rad; 1:5000 in TBS-T) for 1 hr. After 4x5min TBS-T washes, detection was performed with chemiluminescence (WestPico Chemiluminescent Substrate; Pierce). Blots were imaged using an Alpha Innotech Fluorchem gel documentation system, and band intensities were analyzed using ImageJ software (NIH).

Supplementary References

Brandao, K.E., M.L. Dell'Acqua, and S.R. Levinson. 2012. A-kinase anchoring protein 150 expression in a specific subset of TRPV1- and CaV 1.2-positive nociceptive rat dorsal root ganglion neurons. *J Comp Neurol*. 520:81-99.

De Jongh, K.S., B.J. Murphy, A.A. Colvin, J.W. Hell, M. Takahashi, and W.A. Catterall. 1996. Specific phosphorylation of a site in the full-length form of the alpha 1 subunit of the cardiac L-type calcium channel by adenosine 3',5'-cyclic monophosphate-dependent protein kinase. *Biochemistry*. 35:10392-402.

Erickson, M.G., B.A. Alseikhan, B.Z. Peterson, and D.T. Yue. 2001. Preassociation of calmodulin with voltage-gated Ca(2+) channels revealed by FRET in single living cells. *Neuron*. 31:973-85.

Erickson, M.G., H. Liang, M.X. Mori, and D.T. Yue. 2003. FRET two-hybrid mapping reveals function and location of L-type Ca2+ channel CaM preassociation. *Neuron*. 39:97-107.

Fuller, M.D., M.A. Emrick, M. Sadilek, T. Scheuer, and W.A. Catterall. 2010. Molecular Mechanism of Calcium Channel Regulation in the Fight-or-Flight Response. *Science Signaling*. 3:ra70.

Gomez, L.L., S. Alam, K.E. Smith, E. Horne, and M.L. Dell'Acqua. 2002. Regulation of A-kinase anchoring protein 79/150-cAMP-dependent protein kinase postsynaptic targeting by

NMDA receptor activation of calcineurin and remodeling of dendritic actin. *J Neurosci*. 22:7027-44.

Graef, I.A., P.G. Mermelstein, K. Stankunas, J.R. Neilson, K. Deisseroth, R.W. Tsien, and G.R. Crabtree. 1999. L-type calcium channels and GSK-3 regulate the activity of NF-ATc4 in hippocampal neurons. *Nature*. 401:703-708.

Hedin, K.E., M.P. Bell, K.R. Kalli, C.J. Huntoon, B.M. Sharp, and D.J. McKean. 1997. Delta-opioid receptors expressed by Jurkat T cells enhance IL-2 secretion by increasing AP-1 complexes and activity of the NF-AT/AP-1-binding promoter element. *J Immunol*. 159:5431-40.

Li, H.M., M.D. Pink, J.G. Murphy, A. Stein, M.L. Dell'Acqua, and P.G. Hogan. 2012. Balanced interactions of calcineurin with AKAP79 regulate Ca2+-calcineurin-NFAT signaling. *Nat Struc Mol Biol*. 19:337-345.

Oliveria, S.F., M.L. Dell'Acqua, and W.A. Sather. 2007. AKAP79/150 anchoring of calcineurin controls neuronal L-type Ca2+ channel activity and nuclear signaling. *Neuron*. 55:261-275.

Sanderson, J.L., J.A. Gorski, E.S. Gibson, P. Lam, R.K. Freund, W.S. Chick, and M.L. Dell'Acqua. 2012. AKAP150-anchored calcineurin regulates synaptic plasticity by limiting synaptic incorporation of Ca2+-permeable AMPA receptors. *J Neurosci*. 32:15036-52.

Tunquist, B.J., N. Hoshi, E.S. Guire, F. Zhang, K. Mullendorff, L.K. Langeberg, J. Raber, and J.D. Scott. 2008. Loss of AKAP150 perturbs distinct neuronal processes in mice. *Proc Natl Acad Sci U S A*. 105:12557-12562.